Published for SISSA by Springer

Received: *June 6, 2022*
Revised: *December 14, 2022*
Accepted: *December 22, 2022*
Published: *January 16, 2023*

Precise predictions for $V + 2$ jet backgrounds in searches for invisible Higgs decays

J.M. Lindert,[a] S. Pozzorini[b] and M. Schönherr[c]

[a] *Department of Physics and Astronomy, University of Sussex, Brighton BN1 9QH, U.K.*
[b] *Physik-Institut, Universität Zürich, CH-8057 Zürich, Switzerland*
[c] *Institute for Particle Physics Phenomenology, Department of Physics, Durham University, Durham, DH1 3LE, U.K.*

E-mail: j.lindert@sussex.ac.uk, pozzorin@physik.uzh.ch, marek.schoenherr@durham.ac.uk

Abstract: We present next-to-leading order QCD and electroweak (EW) theory predictions for $V + 2$ jet production, with $V = Z, W^{\pm}$, considering both the QCD and EW production modes and their interference. We focus on phase-space regions where $V + 2$ jet production is dominated by vector-boson fusion, and where these processes yield the dominant irreducible backgrounds in searches for invisible Higgs boson decays. Predictions at parton level are provided together with detailed prescriptions for their implementation in experimental analyses based on the reweighting of Monte Carlo samples. The key idea is that, exploiting accurate data for $W + 2$ jet production in combination with a theory-driven extrapolation to the $Z + 2$ jet process can lead to a determination of the irreducible background at the few-percent level. Particular attention is devoted to the estimate of the residual theoretical uncertainties due to unknown higher-order QCD and EW effects and their correlation between the different $V + 2$ jet processes, which is key to improve the sensitivity to invisible Higgs decays.

Keywords: Electroweak Precision Physics, Higher Order Electroweak Calculations

ArXiv ePrint: 2204.07652

https://doi.org/10.1007/JHEP01(2023)070

JHEP01(2023)070

Contents

1 Introduction

Along the main objectives of current and future runs of the Large Hadron Collider (LHC) will be a further detailed investigation of the Higgs sector and the search for physics beyond the Standard Model (BSM). In fact, these two objects are linked, since very precise measurements of Higgs couplings and properties might reveal hints of BSM physics. A prime example of this is given by the branching ratio of the Higgs boson into invisible particles. In the Standard Model (SM), the only invisible decay mode of the Higgs boson proceeds via $H \to ZZ^* \to 4\nu$, with a branching ratio of only about 10^{-3} [1]. In various extensions of the SM this invisible branching ratio can be strongly enhanced [2–4], in particular in scenarios where the Higgs boson can decay into a pair of weakly interacting massive particles — prime candidates of particle dark matter [5–10] (for a recent review see ref. [11]). Therefore, experimental limits on invisible Higgs decays ($H \to \text{inv}$) can be used to exclude regions of parameter space of these models. At the LHC any production mode where the Higgs boson is produced in association with visible SM particles can in principle be used in order to search for $H \to \text{inv}$. Most stringent bounds have been obtained combining searches in Higgs production via vector-boson fusion (VBF) and Higgs production in association with a vector boson (VH) performed by both ATLAS [12–15] and

CMS [16–19]. These searches yield as currently best limit on the invisible Higgs branching ratio $\mathrm{Br}(H \to \mathrm{inv}) < 0.18$ at 95% confidence level [19]. The sensitivity is dominated by the VBF channel, where invisible Higgs searches are based on measurements of the distribution in the dijet invariant-mass, m_{jj}, in the TeV region. The signature of two forward jets with large m_{jj} together with sizeable missing transverse energy receives large contributions from irreducible SM backgrounds, originating in particular from Z-boson production and decay into neutrinos in association with two jets. For this reason, significant sensitivity improvements in $H \to \mathrm{inv}$ searches can be achieved by controlling these backgrounds at the percent level. This in turn becomes possible via a theory assisted data-driven strategy, where precision measurements are combined with state-of-the-art theoretical predictions for Z+2 jet and W+2 jet distributions and for their ratios. Using this approach for the V+jet backgrounds to monojet signals [20] made it possible to enhance the sensitivity of dark-matter searches at the LHC in a very significant way [21, 22].

Besides controlling backgrounds in $H \to \mathrm{inv}$ searches, $V + 2$ jet production is of importance and relevance in its own right. It serves as a laboratory for QCD dynamics and can be used to derive stringent bounds on anomalous triple gauge boson couplings and corresponding dimension-6 effective field theory coefficients [23–27]. In regard of the former, VBF production of vector bosons, which contributes to $V + 2$ jet production at large dijet invariant mass and/or rapidity separation, can provide important insights for the understanding of the QCD dynamics in vector boson scattering (VBS) processes.

In this paper we present new theory predictions for $V + 2$ jet production, with $V = Z, W^{\pm}$, including next-to-leading order (NLO) QCD and electroweak (EW) corrections together with detailed recommendations for their implementation for improving $V + 2$ jet backgrounds in searches for invisible Higgs decays. When referring to $W + 2$ jet and $Z + 2$ jet production, we mean, respectively, the full $2 \to 4$ off-shell proceeses $pp \to \ell^+\nu_\ell/\nu_\ell\ell^- + 2$ jets and $pp \to \ell^+\ell^-/\nu_\ell\bar{\nu}_l + 2$ jets, where $\ell^{\pm} = e^{\pm}$ or $\mu^{\pm}$, lepton/neutrino pairs are produced via $W^{\pm}$ or Z/γ^* vector-boson exchange. Since invisible Higgs searches via VBF at the LHC are based on the m_{jj} distribution, the main focus of this paper is on this particular observable.

At leading order (LO), $V + 2$ jet final state can be generated through a QCD production mode of order[1] $\alpha_s^2\alpha^2$, an EW production mode of order α^3, and QCD-EW interference effects of order $\alpha_s\alpha^3$. The EW production mode receives contributions from VBF-type production as well as from diboson production with subsequent semi-leptonic decays, and in the case of $W + 2$ jets also from single-top production with leptonic decays. At NLO four perturbative terms of order $\alpha_s^{3-n}\alpha^{2+n}$ with $n = 0, 1, 2, 3$ emerge. The contributions of order $\alpha_s^3\alpha^2$ and $\alpha_s^2\alpha^3$ will be referred to as QCD and EW corrections to the QCD production mode, respectively, while terms of order $\alpha_s\alpha^4$ and α^5 will be denoted as the QCD and EW corrections to the EW production mode. In this study we present predictions for all of these LO and NLO contributions, considering $pp \to W^{\pm} + 2$ jets and $pp \to Z + 2$ jets including off-shell leptonic decays and invisible decays in the case of $Z + 2$ jet production. We critically investigate remaining higher-order uncertainties at the NLO level and their correlation between the different $V + 2$ jet processes. To this end we consider besides remaining QCD

[1] Here and in the following we include a factor α stemming from vector-boson decays.

and EW uncertainties also uncertainties due to missing mixed QCD-EW corrections and due to the matching to parton showers (PS). For the implementation of our theoretical predictions in the framework of invisible Higgs searches we propose a procedure based on the reweighting of Monte Carlo samples with perturbative predictions for the $m_{\rm jj}$ distribution, providing also detailed prescriptions for the estimate of theoretical uncertainties including correlations between the $Z + 2\,$jet and $W + 2\,$jet processes.

The NLO QCD corrections to the $V + 2\,$jet QCD production modes are widely available [28–30] (for $pp \to V + n$ jets with $n > 2$ see e.g. [31–37]) and even next-to-next-to leading order (NNLO) corrections are within reach [38, 39]. The NLO QCD corrections to the QCD modes are readily available within general purpose shower Monte Carlo (SMC) programs [40–43], where they typically enter Monte Carlo samples when NLO predictions for $V + 0, 1, 2$ jets production are merged and combined with parton showers at NLO [44–47]. Additionally, logarithmically enhanced corrections beyond fixed-order NLO due to wide-angle QCD emissions are available [48–50]. NLO EW corrections to the QCD modes of $V + 2\,$jet production are known at fixed-order [51–54] and have also been combined with a QCD+QED parton shower using an approximation where only subleading QED effects are neglected [53]. The QCD corrections to the EW modes are only known in the so-called *VBF approximation*, where the VBF subprocess alone is considered, and the cross-talk between quark lines is neglected in the higher-order corrections [55, 56]. Within this approximation NLO QCD corrections to the EW modes have been matched to parton showers [57, 58]. Full NLO QCD+EW predictions for both $pp \to V + 2\,$jets processes in the EW production mode beyond the VBF approximation are presented for the first time in this paper. Similar predictions for $pp \to W^\pm + 2\,$jets have been presented in ref. [59] for a phase-space region dominated by single-top production.

The paper is organised as following. In section 2 we discuss the structure of the NLO corrections to $V + 2\,$jet production considering both the QCD and EW production modes and their interference. In section 3 we propose a reweighting procedure for the incorporation of the higher-order corrections into Monte Carlo samples. Theoretical predictions and uncertainties are presented in section 4, and our conclusions can be found in section 5.

2 $V + 2\,$jet QCD and EW production modes at NLO

We consider the processes $pp \to V + 2\,$jets with

$$V = \begin{cases} Z^\nu & \text{for} \quad pp \to Z(\nu_\ell \bar{\nu}_\ell) + 2\,\text{jets} \\ Z^\ell & \text{for} \quad pp \to Z/\gamma^*(\ell^+\ell^-) + 2\,\text{jets} \\ W^\pm & \text{for} \quad pp \to W^\pm(\ell^\pm \nu_\ell) + 2\,\text{jets} \end{cases} \tag{2.1}$$

where $\ell = e$ or μ. At LO such processes receive three perturbative contributions as illustrated in the top row of figure 1. Thus, the total LO differential cross section in a certain observable x can be written as

$$\frac{\mathrm{d}}{\mathrm{d}x}\sigma^V_{\rm LO} = \frac{\mathrm{d}}{\mathrm{d}x}\sigma^{V,\rm QCD}_{\rm LO} + \frac{\mathrm{d}}{\mathrm{d}x}\sigma^{V,\rm EW}_{\rm LO} + \frac{\mathrm{d}}{\mathrm{d}x}\sigma^{V,\rm interf}_{\rm LO}\,. \tag{2.2}$$

JHEP01(2023)070

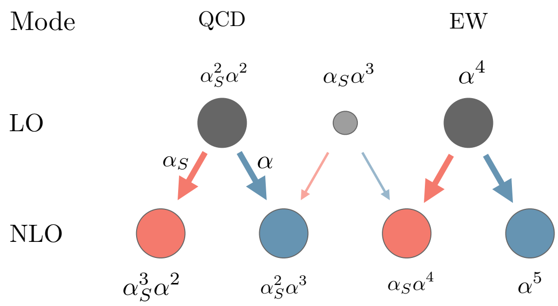

Figure 1. Tower of perturbative contributions to $V + 2\,$jet production at LO and NLO considered and evaluated in this study. In the presented counting the $\mathcal{O}(\alpha)$ vector-boson decays are included.

The *QCD mode* contributes at $\mathcal{O}(\alpha_s^2\alpha^2)$ and consists of absolute squares of the coherent sum of diagrams of $\mathcal{O}(g_s^2e^2)$, exemplified by figures 2(a) and 2(b). The *EW mode*, on the other hand, contributes at $\mathcal{O}(\alpha^4)$ and comprises the absolute square of the coherent sum of all diagrams of $\mathcal{O}(e^4)$, see figures 2(e)–2(l) for example diagrams. Their *interference* contribution at $\mathcal{O}(\alpha_s\alpha^3)$ then is mostly comprised of the interference of $\mathcal{O}(g_s^2e^2)$ diagrams with $\mathcal{O}(e^4)$ diagrams. It, however, also contains genuine contributions consisting of absolute squares of $\mathcal{O}(g_se^3)$ diagrams, for an example see figures 2(c) and 2(d), typically containing an external gluon and an external photon. Partonic channels with initial- or final-state photons are systematically included wherever they contribute at the given perturbative order. In particular, in order to facilitate the cancellation of collinear singularities at NLO QCD+EW, we use a democratic jet clustering algorithm, where photons, quarks and gluons are treated on the same footing as jet constituents.[2]

The contributions to the EW mode (and consequently also to the interference) deserve some closer inspection. Diagrams illustrated in figures 2(e) and 2(f), contribute to VBF-type production, while diagrams as in figures 2(g) and 2(h) contribute to (off-shell) diboson production with one vector boson decaying hadronically and the other leptonically. In the literature these are often denoted as t-channel and s-channel contributions, respectively. In general, partonic channels with qq' initial states involve EW Feynman diagrams with t-channel and/or u-channel exchange of vector bosons. In the case of $q\bar{q}'$ channels also diagrams with s-channel vector boson exchange contribute. The widely used VBF approximation is a gauge-invariant prescription that isolates only squared t-channel and u-channel contributions discarding their interference as well as any s-channel diagram. In this approximation, the final-state vector boson can couple either to an external quark line or to the vector boson that is exchanged in the t/u-channel as in figures 2(e) and 2(f), respectively.

In addition, the EW mode also features photon-induced processes, see figure 2(i). Since we employ the five-flavour (5F) number scheme throughout, b-quarks are treated as massless partons, and channels with initial-state b-quarks are taken into account for all processes and perturbative orders. In the 5F scheme, the process $pp \to W + 2\,$jets includes partonic channels of type $qb \to q'bW$ that involve EW topologies corresponding to t-channel single-top production, $qb \to q't(bW)$, as illustrated in figure 2(k). Top resonances

[2] For technical details concerning the treatment of jets and photons see sections 3.2 and 4.1.

JHEP01(2023)070

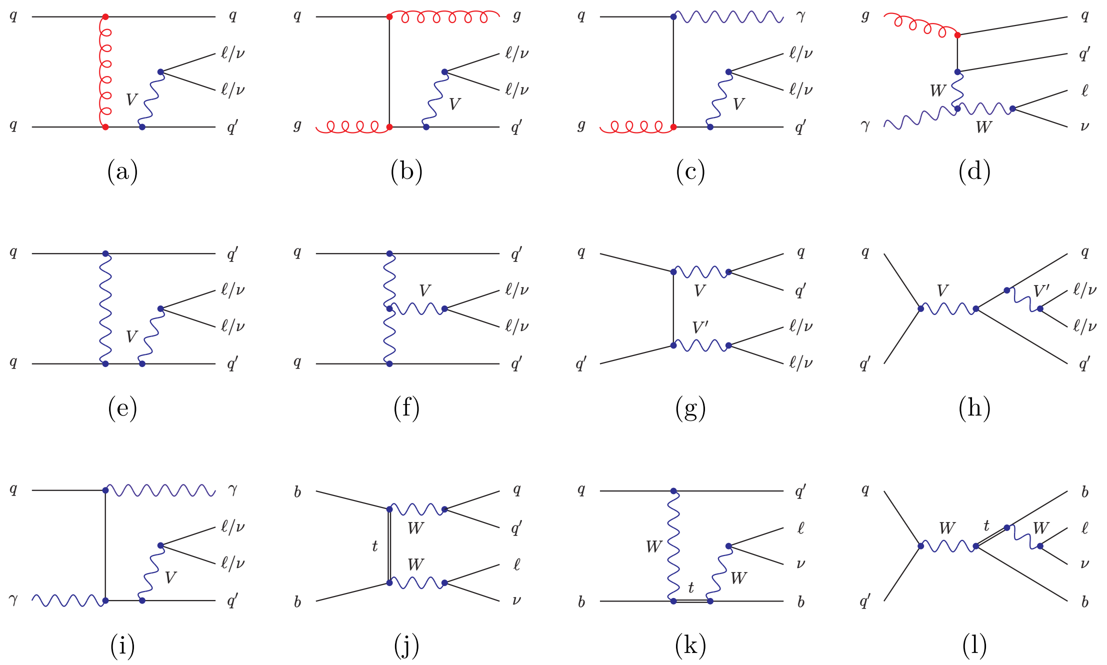

Figure 2. Example LO diagrams at $\mathcal{O}(g_s^2 e^2)$ (a,b), $\mathcal{O}(g_s e^3)$ (c,d), and $\mathcal{O}(e^4)$ (e-l). The square of $\mathcal{O}(g_s^2 e^2)$ diagrams yields the $\mathcal{O}(\alpha_s^2 \alpha^2)$ QCD LO amplitude, while the square of the $\mathcal{O}(e^4)$ diagrams yields the $\mathcal{O}(\alpha^4)$ EW LO amplitude. The $\mathcal{O}(\alpha_s \alpha^3)$ perturbative contribution emerges as square of $\mathcal{O}(g_s e^3)$ diagrams, or due to the interference between $\mathcal{O}(g_s^2 e^2)$ and $\mathcal{O}(e^4)$ diagrams.

occur also in light-flavour channels of type $q\bar{q}' \to \bar{b}bW$, which receive contributions from s-channel single-top production, $q\bar{q}' \to \bar{b}t(bW)$, illustrated in figure 2(l). All these single-top contributions are consistently included in our predictions. When the dijet invariant mass, $m_{\mathrm{j_1j_2}}$, is well below the TeV scale, their numerical impact can yield a substantial fraction of the total EW $W + 2\,$jet cross section at LO. For example, the combined t-channel and s-channel $pp \to tj$ processes yields around 25% of the total EW $W + 2\,$jet process at $m_{\mathrm{j_1j_2}} = 500\,\mathrm{GeV}$. At higher $m_{\mathrm{j_1j_2}}$ the impact of the single-top modes is increasingly suppressed, and for $m_{\mathrm{j_1j_2}} > 2.5\,\mathrm{TeV}$ it is below 1% of the EW $W + 2\,$jet process. More details on the impact of single-top contributions can be found in section 4.2.1.

The LO interferences between QCD and EW modes that contribute at $\mathcal{O}(\alpha_s \alpha^3)$ are largely colour suppressed and yield very small contributions. This in particular holds in the VBF phase space, i.e. with large dijet invariant masses and large rapidity separation of the leading jets. We will highlight the quantitative impact of the interference contributions explicitly in section 4.2.1. In experimental searches for invisible Higgs decays this interference contribution should be considered as separate background (or as an additional systematic uncertainty) besides the QCD and EW $V + 2\,$jet modes, independent between $pp \to Z(\nu_\ell \bar{\nu}_\ell) + 2\,$jets and $pp \to W^{\pm}(\ell^{\pm}\nu_\ell) + 2\,$jets.

As illustrated in figure 1 (bottom row) at NLO four perturbative contributions emerge. Out of these only the contribution with the highest and lowest power of α_s, i.e. the ones of $\mathcal{O}(\alpha_s^3 \alpha^2)$ and $\mathcal{O}(\alpha^5)$, can unambiguously be considered as, respectively, QCD corrections to the QCD mode and EW corrections to the EW mode. The contributions of $\mathcal{O}(\alpha_s^2\alpha^3)$ and $\mathcal{O}(\alpha_s\alpha^4)$ will be referred to, respectively, as the NLO EW corrections to the QCD mode and NLO QCD corrections to the EW mode. However one should keep in mind that $\mathcal{O}(\alpha_s^2\alpha^3)$ and $\mathcal{O}(\alpha_s\alpha^4)$ terms also involve, respectively, QCD and EW corrections to the LO QCD-EW interference. In the literature the $\mathcal{O}(\alpha_s\alpha^4)$ corrections have been often computed in the VBF approximation [55], where, similarly as in the LO case, only squared t- or u-channel contributions are included, and colour exchange between the two quark lines is neglected.

In this paper we present the first complete computation of the NLO QCD+EW corrections to EW $Z+2\,$jet and $W+2\,$jet production. This computation takes into account any contribution at the given perturbative orders, including any relevant cross-talk between different quark lines, t-, u-, and s-channel contributions and their interference, interference effects between the QCD and EW modes, as well as s-channel and t-channel single-top contribution in the case of EW $W^\pm(\ell^\pm\nu_\ell)+2\,$jets production. Therefore, this computation can be seen as a unified NLO description of VBF vector-boson production, vector-boson pair-production with semi-leptonic decays and, in the case of $W^\pm(\ell^\pm\nu_\ell)+2\,$jets production, t-channel plus s-channel single-top production.

In $W+2\,$jet production at $\mathcal{O}(\alpha_s\alpha^4)$, top resonances occur, besides in t-channel and s-channel configurations, also in channels of type $gb\to Wbq\bar{q}'$, which involve Wt-channel single-top production, $gb\to Wt(bq\bar{q}')$. We have verified that these contributions are always at or significantly below the 1% level with respect to the EW LO mode for all considered observables. For $m_{\mathrm{j_1j_2}}>2\,$TeV these contributions are suppressed to below the permil level.

The total differential NLO cross section for $pp\to V+2\,$jet production in a certain observable x can be written as

$$\frac{\mathrm{d}}{\mathrm{d}x}\sigma^{V}_{\mathrm{NLO}}=\frac{\mathrm{d}}{\mathrm{d}x}\sigma^{V,\mathrm{QCD}}_{\mathrm{NLO\,QCD+EW}}+\frac{\mathrm{d}}{\mathrm{d}x}\sigma^{V,\mathrm{EW}}_{\mathrm{NLO\,QCD+EW}}+\frac{\mathrm{d}}{\mathrm{d}x}\sigma^{V,\mathrm{interf}}_{\mathrm{LO}}\,, \tag{2.3}$$

where

$$\frac{\mathrm{d}}{\mathrm{d}x}\sigma^{V,M}_{\mathrm{NLO\,QCD+EW}}=\frac{\mathrm{d}}{\mathrm{d}x}\sigma^{V,M}_{\mathrm{LO}}+\frac{\mathrm{d}}{\mathrm{d}x}\delta\sigma^{V,M}_{\mathrm{NLO\,QCD}}+\frac{\mathrm{d}}{\mathrm{d}x}\delta\sigma^{V,M}_{\mathrm{NLO\,EW}}\,, \tag{2.4}$$

and $M=\{\mathrm{QCD},\mathrm{EW}\}$ identifies the corresponding production mode. The NLO QCD and NLO EW corrections $\delta\sigma^{V,M}_{\mathrm{NLO\,QCD}}$ and $\delta\sigma^{V,M}_{\mathrm{NLO\,EW}}$ correspond to the perturbative contributions of $\mathcal{O}(\alpha_s^3\alpha^2)$ and $\mathcal{O}(\alpha_s^2\alpha^3)$ for $M=\mathrm{QCD}$, and of $\mathcal{O}(\alpha_s\alpha^4)$ and $\mathcal{O}(\alpha^5)$ for $M=\mathrm{EW}$. For later convenience we also define pure NLO QCD predictions without EW corrections,

$$\frac{\mathrm{d}}{\mathrm{d}x}\sigma^{V,M}_{\mathrm{NLO\,QCD}}=\frac{\mathrm{d}}{\mathrm{d}x}\sigma^{V,M}_{\mathrm{LO}}+\frac{\mathrm{d}}{\mathrm{d}x}\delta\sigma^{V,M}_{\mathrm{NLO\,QCD}}\,, \tag{2.5}$$

and pure NLO EW predictions without QCD corrections,

$$\frac{\mathrm{d}}{\mathrm{d}x}\sigma^{V,M}_{\mathrm{NLO\,EW}}=\frac{\mathrm{d}}{\mathrm{d}x}\sigma^{V,M}_{\mathrm{LO}}+\frac{\mathrm{d}}{\mathrm{d}x}\delta\sigma^{V,M}_{\mathrm{NLO\,EW}}\,. \tag{2.6}$$

As a natural approximation of mixed QCD-EW higher-order corrections we also define a factorised combination of NLO QCD and NLO EW corrections,

$$\frac{\mathrm{d}}{\mathrm{d}x}\sigma^{V,M}_{\mathrm{NLO\,QCD\times EW}}=\frac{\mathrm{d}}{\mathrm{d}x}\sigma^{V,M}_{\mathrm{NLO\,QCD}}\left(1+\kappa^{V,M}_{\mathrm{EW}}(x)\right)\,, \tag{2.7}$$

with the NLO EW correction factors

$$\kappa_{\text{EW}}^{V,M}(x) = \frac{\frac{\text{d}}{\text{d}x}\delta\sigma_{\text{NLO EW}}^{V,M}}{\frac{\text{d}}{\text{d}x}\sigma_{\text{LO}}^{V,M}}\,. \tag{2.8}$$

3 Reweighting of Monte Carlo samples

Since the matching of fully off-shell NLO QCD+EW calculations to parton showers for $pp \to V + 2\,\text{jets}$ is beyond reach of the present matching techniques, the reweighting of (N)LO QCD Monte Carlo (MC) samples with NLO QCD+EW parton-level predictions is the natural alternative to enable state-of-the art theory accuracy in the context of invisible-Higgs searches. To this end, in following we define a MC reweighting procedure for the individual QCD and EW production modes in $pp \to V + 2\,\text{jet}$, and we introduce a systematic approach to handle perturbative and MC uncertainties as well as their correlations.

For practical purposes the reweighting has to be performed based on a one-dimensional distribution in a certain observable x. The relevant higher-order theory (TH) predictions for this observable are defined as

$$\frac{\text{d}}{\text{d}x}\sigma_{\text{TH}}^{V,M}\left(\vec{\varepsilon}_{\text{TH}}^{\,V,M}\right) = \int \text{d}\mathbf{y}\,\theta_{\text{cuts}}^{V}(\mathbf{y})\,\frac{\text{d}}{\text{d}x}\frac{\text{d}}{\text{d}\mathbf{y}}\,\sigma_{\text{TH}}^{V,M}\left(\vec{\varepsilon}_{\text{TH}}^{\,V,M}\right)\,, \tag{3.1}$$

where V indicates the specific $V + 2\,\text{jet}$ process in eq. (2.1), and $M = \text{QCD}, \text{EW}$ identifies the corresponding production mode. Since LHC searches for invisible Higgs decays in the VBF channel are based on measurements of the dijet invariant-mass distribution, as reweighting observable we choose

$$x = m_{\text{j}_1\text{j}_2}\,, \tag{3.2}$$

where $m_{\text{j}_1\text{j}_2}$ is the dijet mass defined in section 3.1. The integration on the r.h.s. of eq. (3.1) involves all degrees of freedom $\mathbf{y}$ that are independent of x. Such degrees of freedom include the fully differential kinematic dependence on the vector-boson decay products and the two leading jets, as well as the QED and QCD radiation that accompanies the VBF production process, i.e. extra jets and photons, and also possible extra leptons and neutrinos from hadron decays.

The function $\theta_{\text{cuts}}^{V}(\mathbf{y})$ on the r.h.s. of eq. (3.1) describes selection cuts for $pp \to V + 2\,\text{jet}$, and the details of its definition (see sections 3.1–3.2) play an important role for the consistent implementation of the MC reweighting procedure. Such cuts are typically chosen in a very similar way for $V = Z, W$, but are not necessarily identical. For instance, in the case $V = W$ the QED radiation from the lepton stemming from the $W \to \ell\nu$ decay is typically subject to a dressing prescription, while dressing is irrelevant for $Z \to \nu\nu$ decays. Note also that the cuts that are applied to the theoretical calculations in eq. (3.1) do not need to be identical to the ones employed in the experimental analysis. They are typically rather similar to the actual experimental cuts but more inclusive.[3]

[3]This is not a necessary prerequisite, i.e. the theoretical cuts $\theta_{\text{cuts}}^{V}(\mathbf{y})$ may be also more exclusive than experimental cuts. The crucial prerequisite is that the MC samples that are going to be reweighted with eq. (3.1) and applied to the experimental analysis should extend over the full phase-space regions that are covered by the theoretical calculations and by the experimental analyses.

JHEP01(2023)070

Theory uncertainties in eq. (3.1) are parametrised through sets of nuisance parameters $\vec{\varepsilon}^{\,V,M}_{\rm TH}$, and variations of individual nuisance parameters in the range

$$\varepsilon^{V,M}_{i,\rm TH} \in [-1,1] \tag{3.3}$$

should be understood as 1σ Gaussian uncertainties.

In a similar way as proposed for monojet dark matter searches [20], the theory predictions for the $V+2\,$jet x-distributions can be embodied into the corresponding MC simulations through a one-dimensional reweighting procedure. In this approach, the reweighted MC samples are defined as

$$\frac{\rm d}{{\rm d}x}\frac{\rm d}{{\rm d}\mathbf{y}}\,\sigma^{V,M}(\vec{\varepsilon}^{\,V,M}_{\rm MC},\vec{\varepsilon}^{\,V,M}_{\rm TH}) := \left[\frac{\frac{\rm d}{{\rm d}x}\sigma^{V,M}_{\rm TH}(\vec{\varepsilon}^{\,V,M}_{\rm TH})}{\frac{\rm d}{{\rm d}x}\sigma^{V,M}_{\rm MC}(\vec{\varepsilon}^{\,V,M}_{\rm MC})}\right]\frac{\rm d}{{\rm d}x}\frac{\rm d}{{\rm d}\mathbf{y}}\,\sigma^{V,M}_{\rm MC}(\vec{\varepsilon}^{\,V,M}_{\rm MC})\,. \tag{3.4}$$

On the r.h.s., $\sigma^{V,M}_{\rm MC}$ with $M=$ QCD, EW correspond to the fully differential $V+2\,$jet Monte Carlo samples before reweighting, and the $\sigma^{V,M}_{\rm MC}$ terms in the numerator and denominator must correspond to the same MC samples used in the experimental analysis. Monte Carlo uncertainties, described by $\vec{\varepsilon}^{\,V,M}_{\rm MC}$, must be correlated in the numerator and denominator, while they can be kept uncorrelated across different processes, apart from $Z(\nu\bar{\nu})+$jets and $Z(\ell\ell)+$jets. As for the $\frac{\rm d}{{\rm d}x}\sigma^{V,M}_{\rm TH}/\frac{\rm d}{{\rm d}x}\sigma^{V,M}_{\rm MC}$ ratio on the r.h.s. of eq. (3.4), it is crucial that the numerator and the denominator are determined using the same definition of the x-distribution, which is provided in sections 3.1–3.2.

The method proposed in [20] foresees the separate reweighting of the various $V+$jet processes, while the correlations between different processes and different x-regions is encoded into the corresponding correlations between nuisance parameters. In this paper we adopt a simplified approach, which is designed for the case where experimental analyses do not exploit theoretical information on the shape of the x-distribution, but only on the correlation between different processes at fixed x. In this case, the relevant information can be encoded into the Z/W ratio

$$R^{Z/W,M}_{\rm TH}(x,\vec{\varepsilon}^{\,Z/W,M}_{\rm TH}) = \frac{\frac{\rm d}{{\rm d}x}\sigma^{Z,M}_{\rm TH}(\vec{\varepsilon}^{\,Z,M}_{\rm TH})}{\frac{\rm d}{{\rm d}x}\sigma^{W,M}_{\rm TH}(\vec{\varepsilon}^{\,W,M}_{\rm TH})}\,, \tag{3.5}$$

where $Z = Z^\nu$ or Z^ℓ, and $W \equiv W^+ + W^-$. The theoretical uncertainties for this ratio are described by a new set of nuisance parameters $\vec{\varepsilon}^{\,Z/W,M}_{\rm TH}$, which account for the various uncertainties of the numerator and denominator, as well as for their correlations. In practice, due to the very similar dynamics of the $Z+2\,$jet and $W+2\,$jet processes, the corresponding uncertainties are strongly correlated. Thus they cancel to a large extent in the ratio. This in particular holds for the uncertainties related to higher-order QCD effects. Our theory predictions to be used for MC reweighting are provided directly at the level of the ratio of eq. (3.5).

This ratio makes it possible to translate the MC prediction for the x-distribution in $W+2\,$jet into a corresponding $Z+2\,$jet prediction,

$$\frac{\rm d}{{\rm d}x}\,\sigma^{Z,M}(\vec{\varepsilon}^{\,W,M}_{\rm MC},\vec{\varepsilon}^{\,Z/W,M}_{\rm TH}) := R^{Z/W,M}_{\rm TH}(x,\vec{\varepsilon}^{\,Z/W,M}_{\rm TH})\,\frac{\rm d}{{\rm d}x}\,\sigma^{W,M}_{\rm MC}(\vec{\varepsilon}^{\,W,M}_{\rm MC})\,. \tag{3.6}$$

Here the idea is that the MC uncertainties in $\sigma^{W,M}_{\mathrm{MC}}$ can be strongly constrained through data, while theory uncertainties are strongly reduced through cancellations in the ratio, which results into an accurate prediction for the x-distribution in $Z + 2$ jets. The latter can be applied to the whole $Z+$ jets sample via reweighting,

$$\frac{\mathrm{d}}{\mathrm{d}x}\frac{\mathrm{d}}{\mathrm{d}\mathbf{y}}\,\sigma^{Z,M}(\vec{\varepsilon}^{\,Z,M}_{\mathrm{MC}},\vec{\varepsilon}^{\,W,M}_{\mathrm{MC}},\vec{\varepsilon}^{\,Z/W,M}_{\mathrm{TH}}) := \left[\frac{\frac{\mathrm{d}}{\mathrm{d}x}\,\sigma^{Z,M}(\vec{\varepsilon}^{\,W,M}_{\mathrm{MC}},\vec{\varepsilon}^{\,Z/W,M}_{\mathrm{TH}})}{\frac{\mathrm{d}}{\mathrm{d}x}\,\sigma^{Z,M}_{\mathrm{MC}}(\vec{\varepsilon}^{\,Z,M}_{\mathrm{MC}})}\right]\frac{\mathrm{d}}{\mathrm{d}x}\frac{\mathrm{d}}{\mathrm{d}\mathbf{y}}\,\sigma^{Z,M}_{\mathrm{MC}}(\vec{\varepsilon}^{\,Z,M}_{\mathrm{MC}})\,. \tag{3.7}$$

Note that the double reweighting procedure defined in eqs. (3.6)–(3.7) is equivalent to a single reweighting of the $Z + 2$ jet x-distribution,

$$\frac{\mathrm{d}}{\mathrm{d}x}\frac{\mathrm{d}}{\mathrm{d}\mathbf{y}}\,\sigma^{Z,M}(\vec{\varepsilon}^{\,Z,M}_{\mathrm{MC}},\vec{\varepsilon}^{\,W,M}_{\mathrm{MC}},\vec{\varepsilon}^{\,Z/W,M}_{\mathrm{TH}}) := \left[\frac{R^{Z/W,M}_{\mathrm{TH}}(x,\vec{\varepsilon}^{\,Z/W,M}_{\mathrm{TH}})}{R^{Z/W,M}_{\mathrm{MC}}(x,\vec{\varepsilon}^{\,Z,M}_{\mathrm{MC}},\vec{\varepsilon}^{\,W,M}_{\mathrm{MC}})}\right]\frac{\mathrm{d}}{\mathrm{d}x}\frac{\mathrm{d}}{\mathrm{d}\mathbf{y}}\,\sigma^{Z,M}_{\mathrm{MC}}(\vec{\varepsilon}^{\,Z,M}_{\mathrm{MC}})\,, \tag{3.8}$$

where $R^{Z/W,M}_{\mathrm{MC}}$ is the MC counterpart of the Z/W ratio defined in eq. (3.5). As discussed above, the definition of the variable x and the binning of its distribution need to be the same in all three terms on the r.h.s. of eq. (3.8). Instead, acceptance cuts must be identical in the numerator and denominator of the double ratio, while particle-level MC predictions can be subject to more exclusive or inclusive cuts in the experimental analysis.

In addition to the cancellation of theoretical uncertainties in the ratio $R^{Z/W,M}_{\mathrm{TH}}$, as discussed above the $W + 2$ jet MC uncertainties can be strongly constrained through data. Moreover, also the $Z + 2$ jet MC uncertainties undergo strong cancellations between the term $\frac{\mathrm{d}}{\mathrm{d}x}\frac{\mathrm{d}}{\mathrm{d}\mathbf{y}}\sigma^{Z,M}_{\mathrm{MC}}(\vec{\varepsilon}^{\,Z,M}_{\mathrm{MC}})$, on the r.h.s. of eq. (3.8), and its integrated counterpart $\frac{\mathrm{d}}{\mathrm{d}x}\sigma^{Z,M}_{\mathrm{MC}}(\vec{\varepsilon}^{\,Z,M}_{\mathrm{MC}})$, which enters the MC ratio $R^{Z/W,M}_{\mathrm{MC}}$ in the denominator. Thus the reweighting procedure eq. (3.8) turns a precise $W + 2$ jet measurement into a precise prediction for $Z + 2$ jets.

The reweighting in eq. (3.8) can be applied to a $Z(\nu_\ell\bar{\nu}_\ell)+2$ jets as well as to a $Z(\ell^+\ell^-)+$ 2 jets MC sample. The former allows to constrain the irreducible backgrounds in Higgs to invisible searches, while the latter allows for validation against data in control regions.

In sections 3.1–3.2 we specify the observables, acceptance cuts, and physics objects relevant for the reweighting in eq. (3.8). The theoretical calculations presented in section 4 are based on these definitions, which need to be adopted also for the MC predictions that enter in the denominator of the double ratio on the r.h.s. of eq. (3.8). The details of this reweighting setup are designed such as to take full advantage of the precision of perturbative calculations, while excluding all effects that are better described by MC simulations (e.g. parton showering, hadronisation, and leptons or missing energy from hadron decays). The described method is intended to guarantee small theoretical uncertainties in phase space regions that are reasonably close (but not identical) to the VBF fiducial region defined employed in the reweighting procedure. For phase-space regions sufficiently different from the VBF selection used in the reweighting dedicated simulations of the higher-order corrections need to be performed.

JHEP01(2023)070

3.1 Observables and cuts

The reweighting in eq. (3.8) should be performed based on the ratio of the one-dimensional distributions in the dijet invariant mass $x = m_{\mathrm{j_1j_2}}$, where $\mathrm{j_1}$ and $\mathrm{j_2}$ are the two hardest jets. The following binning is adopted for distributions in $m_{\mathrm{j_1j_2}}$

$$\frac{m_{\mathrm{j_1j_2}}}{\mathrm{GeV}} \in [500, 550, \ldots, 950, 1000, 1100, \ldots, 1900, 2000, 2500, 3000, 3500, 4000, 6000, 13000]\,. \tag{3.9}$$

Theoretical predictions for the $m_{\mathrm{j_1j_2}}$-distribution and their MC counterpart should be determined in the presence of the following cuts,

$$\begin{aligned} &p_{\mathrm{T,j_1}} > 100\,\mathrm{GeV}\,, \qquad p_{\mathrm{T,j_2}} > 50\,\mathrm{GeV}\,, \qquad m_{\mathrm{j_1j_2}} > 500\,\mathrm{GeV}\,, \qquad \Delta\eta_{\mathrm{j_1j_2}} > 2.5\,,\\ &p_{\mathrm{T},V} > 150\,\mathrm{GeV}\,, \end{aligned} \tag{3.10}$$

for $V = W^\pm, Z$. The relevant definitions of jets and $p_{\mathrm{T},V}$ are discussed in section 3.2. Note that only the reconstructed vector-boson momenta are subject to cuts, while no restriction is applied to the individual momenta of their decay products. For $pp \to \ell\ell + 2\,\mathrm{jets}$ the additional process-specific cut

$$m_{\ell\ell} > 40\,\mathrm{GeV} \tag{3.11}$$

should be applied.

For a realistic assessment of theoretical uncertainties one should also consider the fact that, within experimental analyses, VBF cuts can be supplemented by a veto on additional jet radiation. In this case we recommend to perform two alternative reweightings with and without jet veto. The difference between MC samples reweighted with jet veto and in the nominal setup of eq. (3.10) should be small and can be taken as an additional uncertainty. In particular we consider an additional veto on jet radiation

$$p_{\mathrm{T,j_3}} < p_{\mathrm{T,cut}} = \max(500\,\mathrm{GeV}, m_{\mathrm{j_1j_2}})/20\,. \tag{3.12}$$

We choose to employ a dynamic jet veto to minimise possible large logarithms that may spoil the perturbative convergence of our results.

Finally, in order to address the limitations of the proposed one-dimensional reweighting in $m_{\mathrm{j_1j_2}}$, we split the phase space into the following three $\Delta\phi_{\mathrm{j_1j_2}}$ regions, where $\Delta\phi_{\mathrm{j_1j_2}}$ is the azimuthal-angle separation between the two leading jets,

$$\Phi_1 = \{\Delta\phi_{\mathrm{j_1j_2}} < 1\}\,, \qquad \Phi_2 = \{1 < \Delta\phi_{\mathrm{j_1j_2}} < 2\}\,, \qquad \Phi_3 = \{2 < \Delta\phi_{\mathrm{j_1j_2}}\}\,. \tag{3.13}$$

These $\Delta\phi_{\mathrm{j_1j_2}}$ bins are motivated by the fact that the higher-order corrections to the reweigthing ratios $R^{Z/W,M}_{\mathrm{TH}}$, defined in eq. (3.5), feature a non-negligible dependence on $\Delta\phi_{\mathrm{j_1j_2}}$. As discussed in section 4.3, this effect is taken into account through a theoretical uncertainty that is derived from the differences between the $R^{Z/W,M}_{\mathrm{TH}}$ ratios in the above $\Delta\phi_{\mathrm{j_1j_2}}$ regions.

3.2 Definition of physics objects

In the following we define the various physics objects relevant for higher-order perturbative calculations and for the reweighting in the Monte Carlo counterparts in eq. (3.8).

JHEP01(2023)070

Neutrinos. In parton-level calculations of $pp \to V + 2\,\text{jet}$, neutrinos originate only from vector-boson decays, while in Monte Carlo samples they can arise also from hadron decays. In order to avoid any bias in the reweighting procedure, only neutrinos arising from Z and W decays at Monte Carlo truth level should be considered.

Charged leptons. Distributions in the lepton p_T and other leptonic observables are known to be highly sensitive to QED radiative corrections, and the differences in the treatment of QED radiation on Monte Carlo and theory side can lead to a bias in the reweighting procedure. To avoid such a bias, dressed leptons should be used, i.e. all leptons are combined with all nearly collinear photons that lie within a cone of

$$\Delta R_{\ell\gamma} = \sqrt{\Delta\phi_{\ell\gamma}^2 + \Delta\eta_{\ell\gamma}^2} < \Delta R_\mathrm{rec}\,. \tag{3.14}$$

For the radius of the recombination cone we employ the standard value $\Delta R_\mathrm{rec} = 0.1$, which allows one to capture the bulk of the collinear final-state radiation, while keeping contamination from large-angle photon radiation from other sources at a negligible level. All lepton observables as well as the kinematics of the reconstructed W and Z bosons are defined in terms of dressed leptons, and, in accordance with standard experimental practice, both muons and electrons should be dressed. In this way differences between electrons and muons, $\ell = e, \mu$, become negligible, and the reweighting function needs to be computed only once for a generic lepton flavour ℓ.

Similarly as for neutrinos, only charged leptons that arise from Z and W decays at Monte Carlo truth level should be considered. Concerning QCD radiation in the vicinity of leptons, no lepton isolation requirement should be imposed in the context of the reweighting procedure. Instead, in the experimental analysis lepton isolation cuts can be applied in the usual manner.

***Z* and *W* bosons.** The off-shell four-momenta of W and Z bosons are defined as

$$\begin{aligned} p^\mu_{W^+} &= p^\mu_{\ell^+} + p^\mu_{\nu_\ell}, \qquad & p^\mu_{W^-} &= p^\mu_{\ell^-} + p^\mu_{\bar\nu_\ell}, \\ p^\mu_Z &= p^\mu_{\ell^+} + p^\mu_{\ell^-}, & p^\mu_Z &= p^\mu_{\nu_\ell} + p^\mu_{\bar\nu_\ell}, \end{aligned} \tag{3.15}$$

where the leptons and neutrinos that result from Z and W decays are defined as discussed above.

Jets. To define jets we use a democratic clustering approach, where quarks, gluons and photons are treated as jet constituents.[4] In a first step, prior to jet clustering, photons are recombined with collinear quarks within $\Delta R_{q\gamma} < \Delta R_\mathrm{rec}$, similarly as for the charged leptons. Subsequently, QCD partons (quarks and gluons) together with the remaining photons are clustered into jets according to the anti-k_T algorithm [60] using R=0.4. As usual, jets are ordered according to their transverse momentum.

Note that democratic jet clustering should be used also in the reweighting procedure, i.e. when evaluating the MC contribution between squared brackets on the r.h.s. of eq. (3.8). However, as discussed in section 3, the reweigthed MC sample can be applied to experimental

[4] Technical subtleties related to the splitting of photons into letpons are discussed in section 4.1.

JHEP01(2023)070

analyses where photons and jets are handled as different objects and are subject to different cuts. In particular, the fact that MC samples implement a fully differential modelling of QED radiation via parton showering makes it possible to apply any desired photon/jet separation after reweighting. For experimental analyses that implement a veto against isolated photons, the potential drawback of our reweighting based on democratic jets lies in the fact that QED parton showering does not provide a reliable description of events with hard isolated photons, which can result in a mismodeling of the related veto efficiency. In order to assess the associated uncertainty we studied the effect of a veto against hard photons with $p_{\mathrm{T}} > 100\,\mathrm{GeV}$ and a minimal ΔR separation of 0.4 with respect to any QCD parton. Such a photon veto acts on subprocesses of type $pp \to Vj\gamma$ and $pp \to V\gamma\gamma$, which contribute to our calculation starting from Born level (in the case of democratic clustering) and including full NLO QCD+EW corrections. Its effect on the reweighting observable, i.e. the Z/W ratio presented in section 4.3, as well as on all observables presented in section 4.2 turns out to be below 1% of the full QCD+EW prediction. This can be regarded as an upper bound for the uncertainty associated with the usage of democratic jet clustering in the reweighting procedure.

We also note that, in principle, our theoretical calculations and the reweighting procedure could be repeated with an alternative definition of jets and photons that is more similar to experimental analyses, where QCD jets and isolated photons are handled as distinct objects and are subject to different cuts. In practice, our calculations can be repeated in the presence of a veto against isolated photons [61]. This would give rise to additional technical subtleties that are related to the cancellation of soft/collinear singularities at NLO QCD+EW. Such subtleties can be addressed using the $q \to \gamma$ [62] and $\gamma \to$jet [63] fragmentation function formalism, which is however currently not available in Sherpa.

4 Theoretical predictions and uncertainties

In this section we present our theoretical input for invisible-Higgs searches. The relevant input parameters are documented in section 4.1, and in section 4.2 we discuss NLO QCD+EW predictions for $pp \to V + 2\,\mathrm{jets}$ at 13 TeV, both at parton level and matched to the parton shower. Our main results for Z/W ratios and their theoretical uncertainties are presented in section 4.3.

All predictions presented in this paper have been obtained within the Sherpa + OpenLoops framework, which supports fully automated NLO QCD+EW calculations at parton level [42, 52, 64] as well as matching [65, 66] to Sherpa's parton shower [67] and multi-jet merging [44] at NLO as implemented in the Sherpa Monte Carlo framework [42, 68–70], which employs Catani-Seymour's dipole subtraction extended to NLO QCD+EW [52, 64, 71–75]. In particular, Sherpa+OpenLoops allows for the simulation of the entire tower of QCD and EW contributions of $\mathcal{O}(\alpha_{\mathrm{s}}^n\alpha^m)$ that are relevant for multi-jet processes like $pp \to V + 2\,\mathrm{jets}$ at LO and NLO. All relevant renormalised virtual amplitudes are provided by the OpenLoops 2 program [76] which implements the techniques of [77, 78] and is interfaced with Collier [79, 80] and OneLOop [81] for the calculation of scalar integrals.

M_W	=	80.399 GeV	Γ_W	=	2.085 GeV
M_Z	=	91.1876 GeV	Γ_Z	=	2.495 GeV
M_H	=	125 GeV	Γ_H	=	4.07 MeV
m_b	=	0 GeV	Γ_b	=	0
m_t	=	172.5 GeV	Γ_t	=	1.32 GeV,
G_μ	=	$1.1663787 \cdot 10^{-5}$ GeV^{-2}			

Table 1. Values of the various physical input parameters. The value of m_b depends on the employed flavour-number scheme as discussed in the text.

4.1 Definition of numerical setup

In the following we specify input parameters and PDFs employed for theoretical predictions in this study. As discussed in section 3, Monte Carlo samples used in the experimental analyses do not need to be generated with the same input parameters and PDFs used for higher-order theoretical predictions.

In the calculation of $pp \to \nu\nu/\ell\nu/\ell\ell + 2\,\text{jets}$ we use the coupling constants, masses and widths as listed in table 1. All unstable particles are treated in the complex-mass scheme [82–84], where width effects are absorbed into the complex-valued renormalised masses

$$\mu_i^2 = M_i^2 - \mathrm{i}\Gamma_i M_i \qquad \text{for} \quad i = \mathrm{W}, \mathrm{Z}, \mathrm{t}. \tag{4.1}$$

The EW couplings are derived from the gauge-boson masses and the Fermi constant G_μ using

$$\alpha = \left| \frac{\sqrt{2}\sin^2\theta_\mathrm{w}\,\mu_W^2 G_\mu}{\pi} \right| , \tag{4.2}$$

and the weak mixing angle θ_w. The latter is determined by

$$\sin^2\theta_\mathrm{w} = 1 - \cos^2\theta_\mathrm{w} = 1 - \frac{\mu_\mathrm{W}^2}{\mu_\mathrm{Z}^2} \tag{4.3}$$

in the complex-mass scheme. The CKM matrix is assumed to be diagonal, and we checked at LO and NLO QCD that for W+2 jet production the difference with respect to a non-diagonal CKM matrix is always well below 1%.

The G_μ-scheme guarantees an optimal description of pure SU(2) interactions at the EW scale as it absorbs universal higher-order corrections to the weak mixing angle into the LO contribution and, thus, minimises higher-order corrections. It is therefore the scheme of choice for W+2 jet production, and it provides a very good description of Z+2 jet production as well. The choice of the G_μ scheme plays an important role also for the cancellation of singularities in partonic subprocesses that involve external photons [85]. In particular, since we treat final-state photons as jet constituents, the real NLO EW corrections involve collinear singularities from massless $\gamma \to q\bar{q}$ splittings, and their cancellation requires that α is renormalised at a finite scale, such as in the G_μ scheme. In the OpenLoops framework, this is automatically ensured by handling photons that are allowed to split into

$q\bar{q}$ pairs as "off-shell photons" as described in Section 3.2 and 3.3 of ref. [76]. Technically, the singularities from real $\gamma \to q\bar{q}$ splittings cancel against $1/\varepsilon$ poles stemming form $\Delta\alpha^{(\text{reg})}(M_Z^2) = \Pi^{\gamma\gamma}_{\text{light}}(0) - \Pi^{\gamma\gamma}_{\text{light}}(M_Z^2)$ in eq. (3.78) of [76]. Note that such $1/\varepsilon$ poles arise from all massless fermions, including leptons. However, $\gamma \to \ell^+\ell^-$ splittings are not included in our calculations, since leptons are not considered as jet constituents. Thus, in order to avoid uncancelled $1/\varepsilon$ poles we have handled leptons as massive fermions in $\Delta\alpha^{(\text{reg})}(M_Z^2)$, while lepton masses have been kept equal to zero anywhere else. The resulting logarithmic terms of type $\ln(m_\ell^2/M_Z^2)$, which result from the fact that $\gamma \to \ell^+\ell^-$ splittings are vetoed in our calculations, amount to a 3% contribution to $\Delta\alpha^{(\text{reg})}(M_Z^2)$. This effect is further suppressed by two orders of magnitude due to the tiny fraction of $V + 2\,$jet events with final-state photons. Thus our results are highly insensitive to the choice of vetoing or not vetoing $\gamma \to \ell^+\ell^-$ splittings.

As renormalisation scale μ_R and factorisation scale μ_F we set

$$\mu_{\text{R,F}} = \xi_{\text{R,F}}\mu_0\,, \quad \text{with} \quad \mu_0 = \frac{1}{2}H'_\text{T} \quad \text{and} \quad \frac{1}{2} \le \xi_\text{R}, \xi_\text{F} \le 2\,. \tag{4.4}$$

Here H'_T is defined as the scalar sum of the transverse energy of all parton-level final-state objects,

$$H'_\text{T} = E_{\text{T},V} + \sum_{i\in\text{partons}} p_{\text{T},i}\,, \quad \text{with} \quad E_{\text{T},V} = \sqrt{m_V^2 + p_{\text{T},V}^2} \tag{4.5}$$

where m_V and $p_{\text{T},V}$ are, respectively, the invariant mass and the transverse momentum of the reconstructed off-shell vector boson momenta as defined in eq. (3.15), while the sum includes all final-state QCD and QED partons (q, g, γ) including those emitted at NLO.[5] Our default scale choice corresponds to $\xi_\text{R} = \xi_\text{F} = 1$, and theoretical QCD scale uncertainties are assessed by applying the standard 7-point variations $(\xi_\text{R}, \xi_\text{F}) = (2,2), (2,1), (1,2), (1,1), (1, \frac{1}{2}), (\frac{1}{2}, 1), (\frac{1}{2}, \frac{1}{2})$.

For the calculation of hadron-level cross sections at NLO(PS) QCD + NLO EW we employ the `NNPDF31_nlo_as_0118_luxqed` PDF set, which encodes QED effects via the LUXqed methodology of [86]. The same PDF set, and the related α_s value, is used throughout, i.e. also in the relevant LO and NLO ingredients used in the estimate of theoretical uncertainties. Consistently with the 5F number scheme employed in the PDFs, b-quarks are treated as massless partons, and channels with initial-state b-quarks are taken into account for all processes and production modes.

In addition to fixed-order calculations including NLO QCD and EW corrections, we also match the NLO QCD corrections to the QCD mode to the QCD parton shower. More precisely, the NLO corrections to $V+2\,$jet production are matched to the QCD parton shower using the S-MC@NLO approach [66]. Here we set the scales according to the CKKW scale setting algorithm of refs. [44, 87], i.e. we interpret the given configuration using the inverse of the parton shower (using only its QCD splitting functions) to arrive at a core process and the reconstructed splitting scales t_i,

$$\alpha_\text{s}^{n+k}(\mu_\text{R}^2) = \alpha_\text{s}^k(\mu_\text{core}^2) \prod_{i=1}^{n} \alpha_\text{s}(t_i)\,. \tag{4.6}$$

[5] This scale choice corresponds to the scale setter `DH_Tp2` in Sherpa.

JHEP01(2023)070

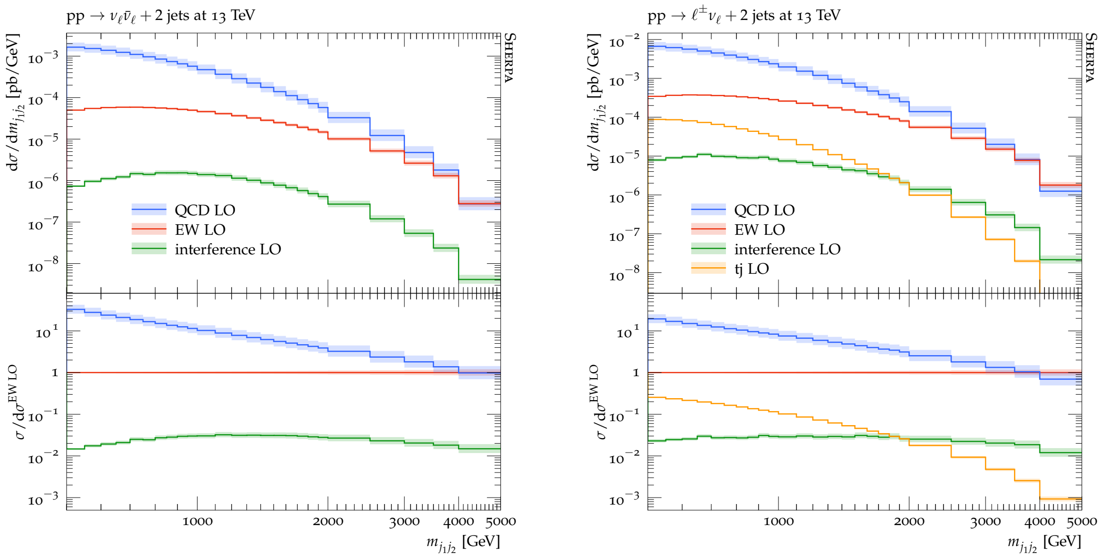

Figure 3. Distribution in the invariant mass of the two hardest jets, $m_{\mathrm{j_1 j_2}}$, for $pp \to Z(\nu_\ell \bar{\nu}_\ell) + 2\,$jets (left) and $pp \to W^\pm(\ell^\pm \nu_\ell) + 2\,$jets (right) at LO. The upper frame shows absolute predictions for the QCD (blue), EW (red), and interference (green) production modes. For $pp \to W^\pm(\ell^\pm \nu_\ell) + 2\,$jets we also show the LO $pp \to tj$ contributions (orange), which belong to the EW production mode and include t-channel and s-channel single-top production. The relative importance of the various contributions normalised to the EW production mode is displayed in the lower frame. The bands correspond to QCD scale variations, and in the case of ratios only the numerator is varied.

We restrict ourselves to strongly ordered hierarchies only, i.e. $\mu_{\mathrm{Q}} > t_1 > t_2 > \ldots > t_n$, as the parton shower would produce them in its regular evolution. In consequence, depending on the phase space point, possible core configurations are $pp \to V$, $pp \to V + j$, $pp \to V + jj$, and $pp \to V + jjj$. Further, we set both the factorisation and the shower starting scale, μ_{F} and μ_{Q} respectively, to the scale $\mu_{\text{core}} = \frac{1}{2}\,H'_{\mathrm{T}}$ defined on the reconstructed core process. In our region of interest where the usual Sudakov factors are negligible, our NLOPS simulation is thus equivalent to the two-jet component of an inclusive NLO merged calculation in the MEPS@NLO algorithm without additional multiplicities merged on top of it.

4.2 Higher-order QCD, EW and PS predictions for $V + 2\,$jet

In this section we present LO and NLO QCD+EW predictions for $pp \to Z(\nu_\ell \bar{\nu}_\ell) + 2\,$jets and $pp \to W^\pm(\ell^\pm \nu_\ell) + 2\,$jets including also parton-shower effects. In the case of $\nu\bar{\nu}$ final states we consider a single generic neutrino flavour $\nu = \nu_e, \nu_\mu$, or ν_τ, as we also do for $\ell \nu_\ell$ final states, where $\ell = e$ or μ. Tau lepton final states are not considered. Since the hard leptons from Z- and W-boson decays are dressed, electrons and muons can be treated on the same footing by neglecting their masses. Each process is split into a QCD and EW production mode as discussed in section 2.

4.2.1 LO contributions and interference

In figure 3 we show LO predictions for $Z + 2\,$jet (left) and $W + 2\,$jet (right) production considering the QCD and EW modes together with the LO interference. In the case of

JHEP01(2023)070

$W+2\,$jet production we also show for illustration purposes the LO contribution due to $pp \to tj$ with leptonic on-shell decays of the top (no such on-shell top approximation is applied within our NLO predictions for $W+2\,$jet). The final-state jet can be a light jet or a bottom-quark jet, i.e. this process comprises t-channel and s-channel single-top production at LO. The single-top processes are consistently included in the off-shell matrix elements of the EW mode of $pp \to W^{\pm}(\ell^{\pm}\nu_\ell)+2\,$jets. For both $Z+2\,$jet and $W+2\,$jet production the QCD mode largely dominates over the EW mode in the bulk of the phase space. However, at large $m_{\mathrm{j_1j_2}}$ the EW mode becomes subsequently more and more important, eventually dominating over the QCD mode for $m_{\mathrm{j_1j_2}} > 4\,$TeV. For both considered processes the LO interference remains more or less constant with respect to the EW mode, at about $2-3\%$ relative to it over the entire $m_{\mathrm{j_1j_2}}$ range. Given the small size of the LO interference contribution, in Higgs to invisible searches it should either be considered as separate background contribution, or taken entirely as additional systematic uncertainty. The $pp \to tj$ process yields around 25% of the total EW $W+2\,$jet process at the lower end of the considered $m_{\mathrm{j_1j_2}}$ range. At large $m_{\mathrm{j_1j_2}}$ the impact of the single-top modes is increasingly suppressed, and for $m_{\mathrm{j_1j_2}} > 2.5\,$TeV it drops below 1% of the EW $W+2\,$jet process.

4.2.2 QCD production

The NLO QCD and EW corrections to the production of $V+2\,$jets via QCD interactions are well known in the literature. For example, ref. [53] presents a systematic investigation of QCD and EW correction effects on high-energy observables. Here we focus on NLO corrections and correlations relevant for invisible-Higgs searches at large invariant masses of the two hardest jets. Besides fixed-order NLO corrections we also investigate the effect of parton-shower matching at NLO QCD.

Figure 4 shows the distribution in $m_{\mathrm{j_1j_2}}$ for $pp \to W^{\pm}(\ell^{\pm}\nu_\ell)+2\,$jets and $pp \to Z(\nu_\ell\bar{\nu}_\ell)+2\,$jets in various approximations. Predictions and scale variations at LO QCD, NLO QCD and NLOPS QCD accuracy are presented together with the additive and multiplicative combination of NLO QCD and EW corrections. For both processes the effect of QCD, EW and shower corrections, as well as the QCD scale variations is remarkably similar.

The impact of QCD corrections is negative, and below 1 TeV it remains quite small, while in the $m_{\mathrm{j_1j_2}}$ tail it becomes increasingly large, reaching around -20% at 2–3 TeV and -50% at 4 TeV. Parton-shower corrections are at the percent level in the $m_{\mathrm{j_1j_2}}$-tail, while below 2 TeV their effect is more sizeable and negative, reaching 20–30% around 500 GeV. This difference between NLO and NLOPS predictions largely exceed the size of QCD scale variations. Thus the latter do not provide a reliable uncertainty estimate at small $m_{\mathrm{j_1j_2}}$. Nevertheless we observe that parton-shower effects in $Z+2\,$jet and $W+2\,$jet production are strongly correlated and cancel to a large extent in the Z/W ratio (see section 4.3). As for the NLO EW corrections, we find an increasingly negative contribution with rising $m_{\mathrm{j_1j_2}}$. Their impact, however, is rather mild and reaches only about -10% in the multi-TeV region.

In figure 5 we show the same $m_{\mathrm{j_1j_2}}$-distributions and theoretical predictions of figure 4 in the presence of the dynamic veto of eq. (3.12) against a third jet. At LO QCD, where only two jets are present, the veto has no effect, while the NLO QCD and NLOPS QCD predictions are strongly reduced. The maximal effect is observed at $m_{\mathrm{j_1j_2}} = 500\,$GeV, where

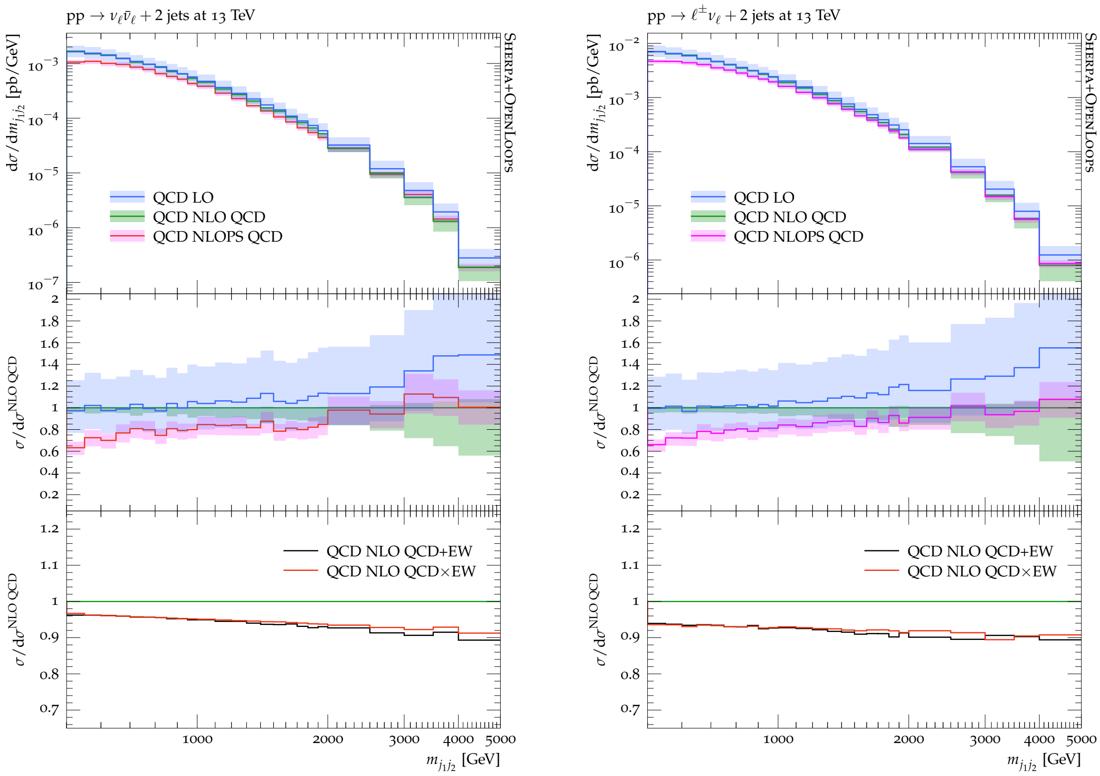

Figure 4. Distribution in the invariant mass of the two hardest jets, $m_{\mathrm{j_1j_2}}$, for QCD $pp \to Z(\nu_\ell\bar{\nu}_\ell) + 2\,\mathrm{jets}$ (left) and QCD $pp \to W^\pm(\ell^\pm\nu_\ell) + 2\,\mathrm{jets}$ (right). The upper frame displays absolute LO QCD (blue), NLO QCD (green), and NLO+PS QCD (magenta) predictions, and ratios with respect to NLO QCD are presented in the central panel. The bands correspond to QCD scale variations, and in the case of ratios only the numerator is varied. The lower panel shows the relative impact of NLO QCD+EW (black) and NLO QCD×EW (red) predictions normalised to NLO QCD.

the veto of eq. (3.12) corresponds to $p_{\mathrm{T,cut}} = 25\,\mathrm{GeV}$, and the NLO QCD cross section is suppressed by a factor four. Above 500 GeV the value of $p_{\mathrm{T,cut}}$ grows linearly with $m_{\mathrm{j_1j_2}}$, and the effect of the veto on the cross section becomes less important. Below 1 TeV the NLO QCD corrections and their scale uncertainties are increasingly large, and scale variations give rise to negative cross sections at $m_{\mathrm{j_1j_2}} \simeq 500\,\mathrm{GeV}$. This is due to the presence of large QCD Sudakov logarithms that arise form the jet veto and need to be resummed by the parton shower. Thus, as far as absolute cross sections are concerned, at small $m_{\mathrm{j_1j_2}}$ fixed-order NLO QCD calculations are not reliable, and only NLOPS predictions can be thrusted. Moreover, the moderate difference between NLO and NLOPS QCD results should be regarded as an accidental agreement due to the choice of the central scale. In fact, as can be seen in figure 5, changing the scale yields much larger NLOPS/NLO differences. At the same time, we note that such differences are dominated by universal Sudakov logarithms that cancel in the ratio between $Z + 2\,\mathrm{jet}$ and $W + 2\,\mathrm{jet}$ cross sections. This is confirmed by the highly universal NLO and NLOPS suppression effects that are observed in $Z + 2\,\mathrm{jet}$ and $W + 2\,\mathrm{jet}$ production. Moreover, we have checked that correlated factor-two scale variations cancel to a large extend in the ratio of m_{jj} distributions for $Z+2\,\mathrm{jet}$ and $W+2\,\mathrm{jet}$

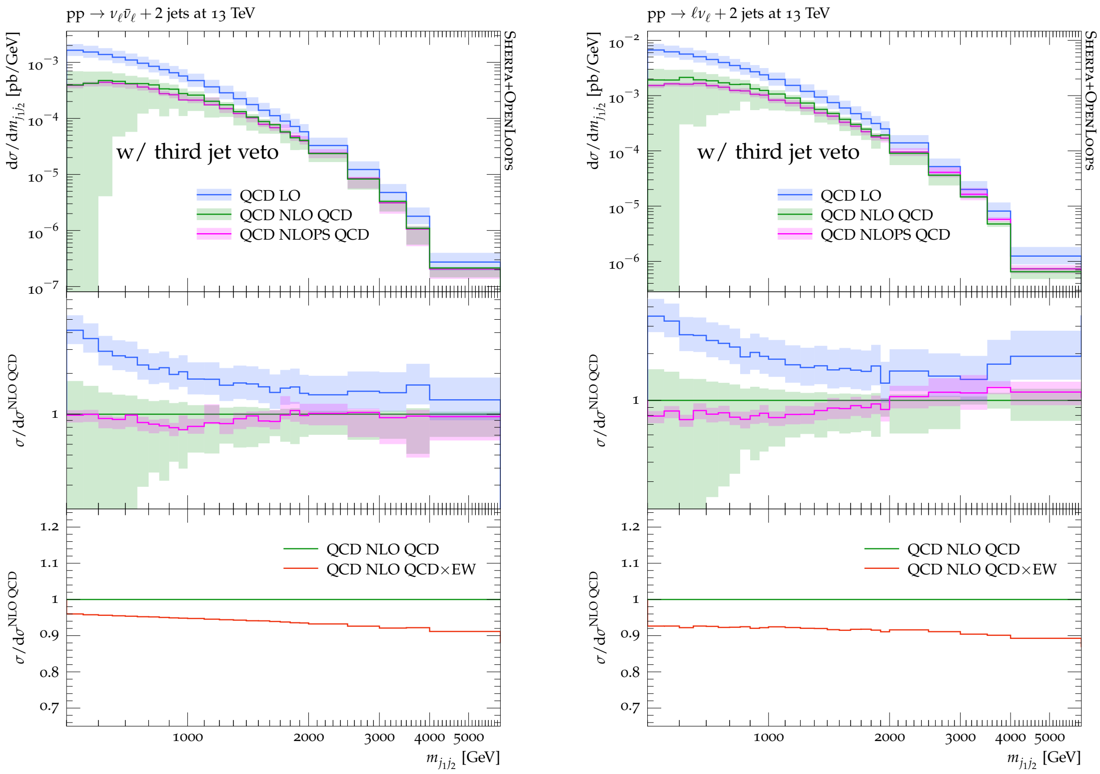

Figure 5. Distribution in the invariant mass of the two hardest jets, $m_{\mathrm{j}_1\mathrm{j}_2}$, for QCD $pp \to Z(\nu_\ell \bar{\nu}_\ell) + 2\,\mathrm{jets}$ (left) and QCD $pp \to W^\pm(\ell^\pm \nu_\ell) + 2\,\mathrm{jets}$ (right) subject to the dynamic veto of eq. (3.12) against a third jet. Curves and bands as in figure 4 but without NLO QCD+EW predictions.

production at NLO QCD. These observations suggest the absence of large higher-order effects beyond NLO in the Z/W ratio.

In figure 5 the EW and QCD corrections are combined using the multiplicative prescription (2.7). This is well justified by the fact that the EW corrections factorise w.r.t. the large QCD Sudakov logarithms that arise form the jet veto, and the resulting EW corrections are almost identical to the inclusive selection. The additive QCD-EW combination is not shown in figure 5 since this prescription is completely unreliable in the presence of a strong jet veto.

4.2.3 EW production

Numerical results for EW $V + 2\,\mathrm{jet}$ production including QCD and EW corrections are shown in figures 6–11. We remind the reader that here we present the first calculation of the complete QCD corrections (beyond the VBF approximation) and of the EW corrections to Z+2 jet production in the EW mode.

In figure 6 differential predictions in the transverse momentum of the (reconstructed) vector bosons, $p_{\mathrm{T},V}$, are shown. We observe that the NLO QCD corrections increase the LO EW cross section by about 20% showing hardly any $p_{\mathrm{T,V}}$ dependence. QCD scale uncertainties at LO are around 10% for small $p_{\mathrm{T},V}$ and increase up to 20% in the tail. The

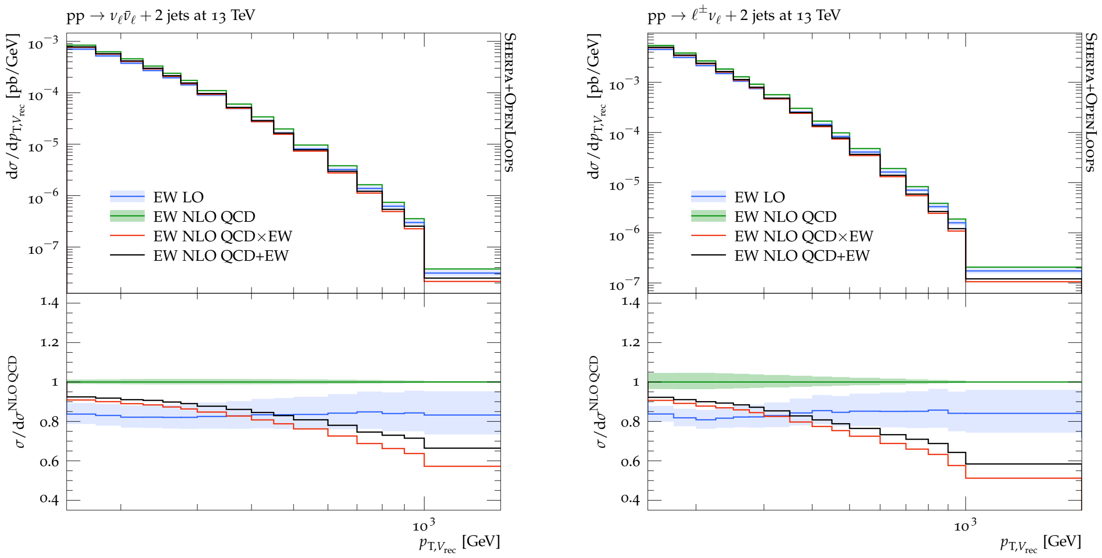

Figure 6. Distribution in the reconstructed transverse momentum of the off-shell vector boson, $p_{\mathrm{T,V}}$, for EW $pp \to Z(\nu_\ell \bar{\nu}_\ell) + 2\,\mathrm{jets}$ (left) and EW $pp \to W^\pm(\ell^\pm \nu_\ell) + 2\,\mathrm{jets}$ (right). Absolute EW LO (blue), NLO QCD (green), NLO QCD+EW (black) and NLO QCD×EW (red) predictions are shown in the upper panel. Here NLO QCD and NLO EW corrections should be understood as $\mathcal{O}(\alpha_s)$ and $\mathcal{O}(\alpha)$ effects w.r.t. to the EW LO. The same predictions normalised to NLO QCD are shown in the lower panel. The bands correspond to QCD scale variations, and in the case of ratios only the numerator is varied.

QCD scale uncertainties at NLO QCD are only at the level of a few percent and decrease to negligible levels in the tail. This is consistent with the computation of the NLO QCD corrections for the $V + 2\,$jet processes in the VBF approximation, where residual scale uncertainties are at the 2% level [55]. Here we note that, given the rather large size of the NLO QCD corrections, such small scale uncertainties cannot be regarded as a reliable estimate of unknown higher-order effects. In the $p_{\mathrm{T,V}}$ distribution the EW corrections display a typical behaviour induced by the dominance of EW Sudakov logarithms. At 1 TeV the EW corrections reduce the NLO QCD cross section by 40–50%, with a spread of about 10% between the additive and the multiplicative combinations. Both QCD and EW corrections are highly correlated between the two considered processes, i.e. the relative impact of these corrections is almost identical.

Higher-order QCD and EW corrections to the transverse momentum distribution of the hardest jet, $p_{\mathrm{T,j_1}}$, are shown in figure 7. Here the QCD corrections are largest at small $p_{\mathrm{T,j_1}}$ and decrease in the tail. For $p_{\mathrm{T,j_1}}$ above a few hundred GeV the NLO QCD corrections drop below 10%. The NLO EW corrections increase logarithmically at large $p_{\mathrm{T,j_1}}$ and reach -40% at 1 TeV. Due to the smallness of the higher-order QCD corrections in the tail, differences between additive and multiplicative combinations are negligible. Again a high degree of correlation of the higher-order corrections is observed between the two processes.

In figures 8 and 9 we turn to the distribution in the invariant mass between of two leading jets, $m_{\mathrm{j_1j_2}}$, defined inclusively and with an additional dynamic veto on central

JHEP01(2023)070

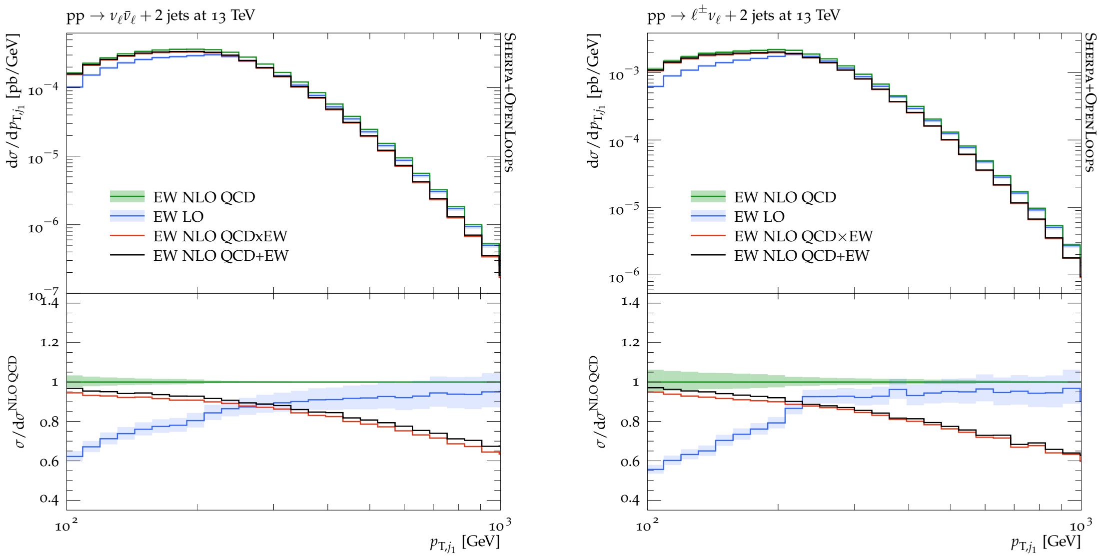

Figure 7. Distribution in the transverse momentum of the hardest jet, $p_{\mathrm{T,j_1}}$, for EW $pp \to Z(\nu_\ell\bar{\nu}_\ell) + 2\,\text{jets}$ (left) and EW $pp \to W^\pm(\ell^\pm\nu_\ell) + 2\,\text{jets}$ (right). Curves and bands as in figure 6.

jet activity as introduced in section 3.1, respectively. These distributions are crucial for background estimations in invisible-Higgs searches. For the jet-inclusive distributions higher-order QCD and EW corrections are highly correlated between the two considered processes with differences at the 5% level for the QCD corrections at small $m_{\mathrm{j_1j_2}}$. At LO QCD, scale uncertainties increase with $m_{\mathrm{j_1j_2}}$ and reach 20–30% in the multi-TeV range. At NLO QCD, scale uncertainties are reduced to the 1% level all the way up to the multi-TeV regime. Overall, the NLO QCD corrections have a marked impact on the shape of the $m_{\mathrm{j_1j_2}}$ distribution, ranging from +70% at small $m_{\mathrm{j_1j_2}}$ to about +5% above 2 TeV. At the same time, NLO EW corrections are negative and increase towards the $m_{\mathrm{j_1j_2}}$ tail. However, they remain smaller compared to the corresponding corrections in $p_{\mathrm{T,V}}$ or $p_{\mathrm{T,j_1}}$. This is due to the fact that, at very large $m_{\mathrm{j_1j_2}}$, the Mandelstam invariants $\hat{t}$ and $\hat{u}$ are much smaller as compared to $\hat{s} \sim m_{\mathrm{j_1j_2}}$. As a consequence the double Sudakov logarithms $\ln^2(|\hat{r}|/M_W^2)$ with $\hat{r} = \hat{t}, \hat{u}$ are significantly suppressed with respect to $\ln^2(\hat{s}/M_W^2)$. At $m_{\mathrm{j_1j_2}} = 5$ TeV the EW corrections amount to about 20%, and differences between an additive and a multiplicative combinations of QCD and EW corrections remain at 1% level. The dynamic central jet veto has marked impact on the NLO QCD corrections, in particular in the small $m_{\mathrm{j_1j_2}}$ region. Here, the corrections are reduced to about +20% for $Z+2\,$jet production, and turn negative to about −20% for $W+2\,$jet production. The dynamic jet veto has a much smaller effect in the TeV regime. Here the QCD corrections for both $Z(\nu_\ell\bar{\nu}_\ell)$ and $W^\pm(\ell^\pm\nu_\ell)$ production are at the percent level only. Unsurprisingly, the EW corrections are hardly effected by the central jet veto.

In figure 10 we plot the differential distribution in the azimuthal separation of the two hardest jets, $\Delta\phi_{\mathrm{j_1j_2}}$. In this observable the EW corrections are at the 10% level with hardly any variation across the $\Delta\phi_{\mathrm{j_1j_2}}$ range. The QCD corrections on the other hand show a mild increase towards smaller $\Delta\phi_{\mathrm{j_1j_2}}$. Interestingly, in this region the QCD

JHEP01(2023)070

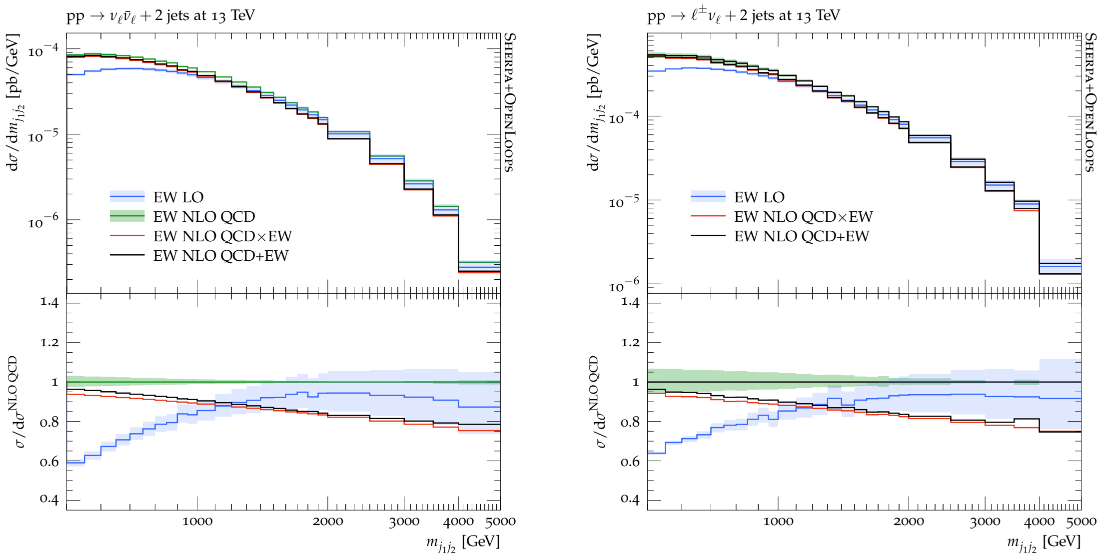

Figure 8. Distribution in the invariant mass of the two hardest jets, $m_{\mathrm{j_1j_2}}$, for EW $pp \to Z(\nu_\ell\bar{\nu}_\ell) + 2\,\mathrm{jets}$ (left) and EW $pp \to W^\pm(\ell^\pm\nu_\ell) + 2\,\mathrm{jets}$ (right). Curves and bands as in figure 6.

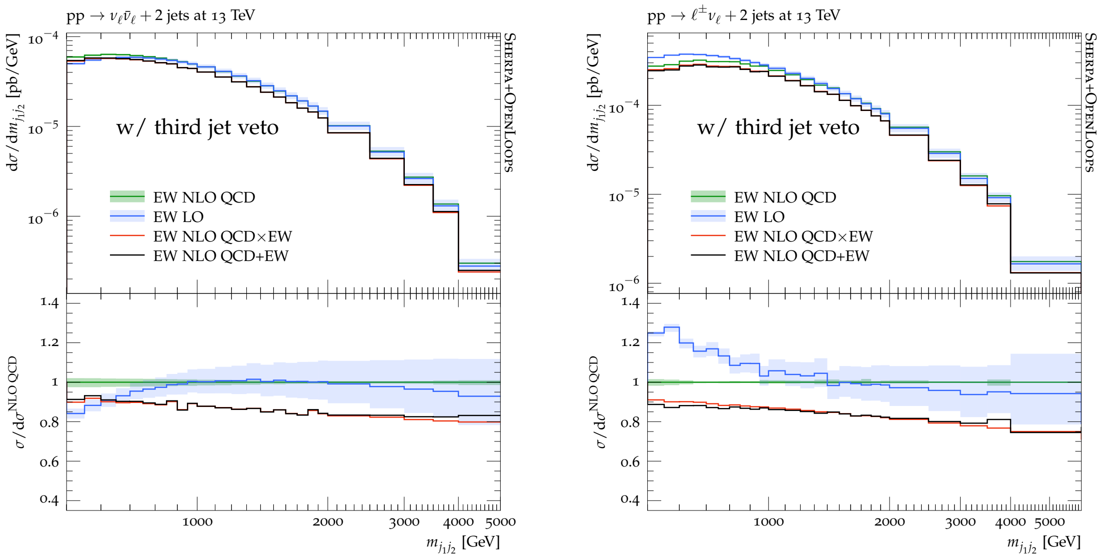

Figure 9. Distribution in the invariant mass of the two hardest jets, $m_{\mathrm{j_1j_2}}$, for EW $pp \to Z(\nu_\ell\bar{\nu}_\ell) + 2\,\mathrm{jets}$ (left) and EW $pp \to W^\pm(\ell^\pm\nu_\ell) + 2\,\mathrm{jets}$ (right) subject to the dynamic third jet veto of eq. (3.12). Curves and bands as in figure 6.

corrections also show a non-universality between the two considered processes at the 10% level. This non-universality can be attributed to the following two mechanisms. The first one is single-top production, which enters only $pp \to W^\pm(\ell^\pm\nu_\ell) + 2\,\mathrm{jets}$ in the form of s- and t-channel contributions at LO and also associated Wt production at NLO QCD (see section 2). The second mechanism consists of s-channel contributions that correspond to diboson subprocesses of type $q\bar{q}' \to VV'$, where one of the weak bosons decays into two jets. At $m_{\mathrm{j_1j_2}} > M_{\mathrm{W,Z}}$, such diboson channels can contribute through hard initial-state radiation,

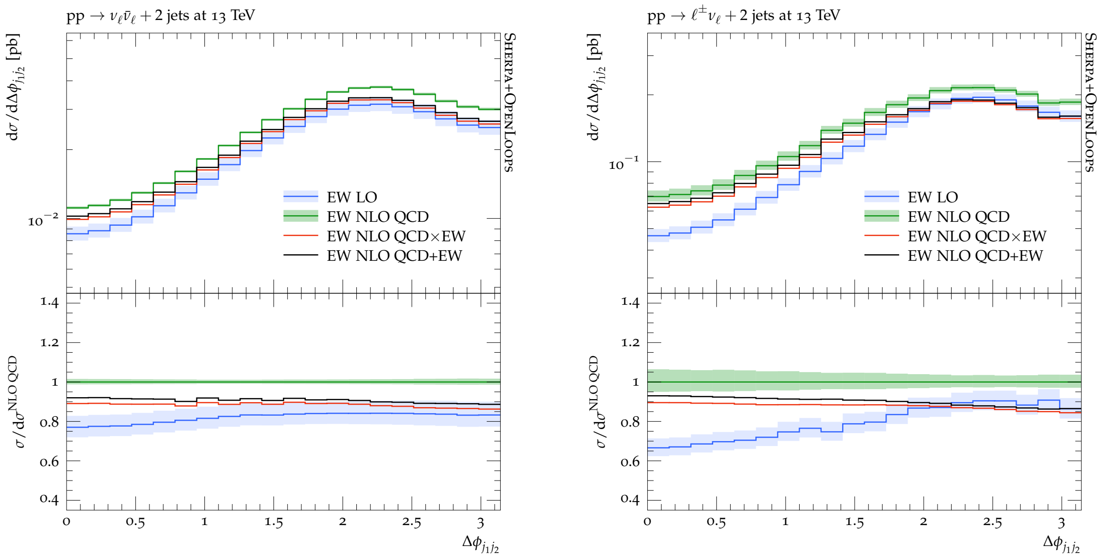

Figure 10. Distribution in the azimuthal separation of the two hardest jets, $\Delta\phi_{\mathrm{j_1 j_2}}$, for EW $pp \to Z(\nu_\ell \bar{\nu}_\ell)+2\,\mathrm{jets}$ (left) and EW $pp \to W^\pm(\ell^\pm \nu_\ell)+2\,\mathrm{jets}$ (right). Curves and bands as in figure 6.

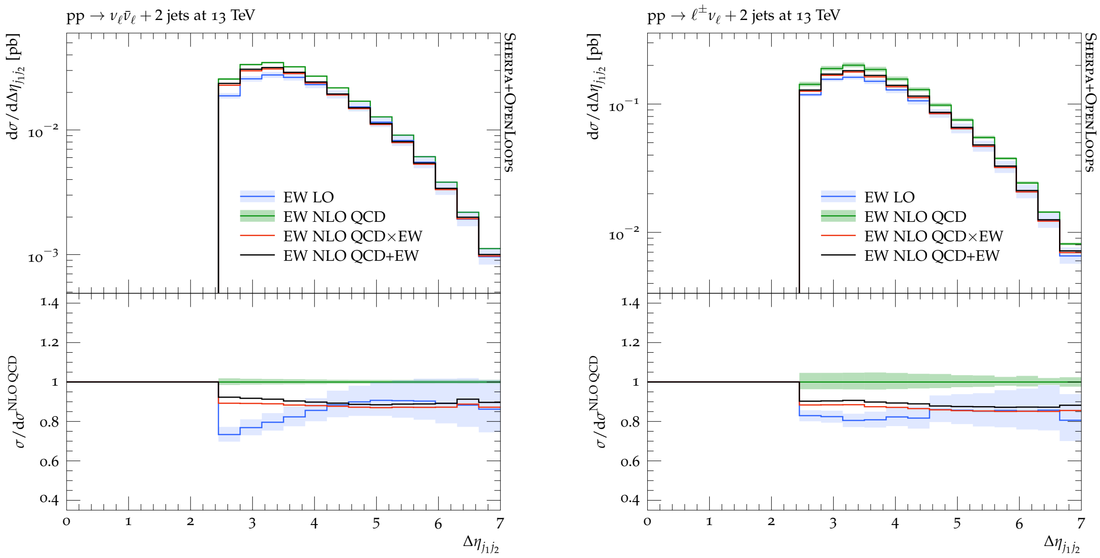

Figure 11. Distribution in the rapidity separation of the two hardest jets, $\Delta\eta_{\mathrm{j_1 j_2}}$, for EW $pp \to Z(\nu_\ell \bar{\nu}_\ell)+2\,\mathrm{jets}$ (left) and EW $pp \to W^\pm(\ell^\pm \nu_\ell)+2\,\mathrm{jets}$ (right). Curves and bands as in figure 6.

which plays the role of one of the two hardest jets. Their non-universality is due to the fact that the QCD corrections to $W^\pm Z$ production are much larger as compared to W^+W^- and ZZ production. Both mechanisms tend to enhance $W^\pm(\ell^\pm \nu_\ell) + 2\,\mathrm{jets}$ production at small $\Delta\phi_{\mathrm{j_1 j_2}}$, while they tend to be suppressed at larger $\Delta\phi_{\mathrm{j_1 j_2}}$. The impact of these mild non-universalities is discussed in more detail in section 4.3.

Finally, in figure 11 we consider the distribution in the rapidity separation of the two hardest jets, $\Delta\eta_{\mathrm{j_1 j_2}}$. Also in this case the EW corrections are almost constant and at the level of 10%. For the $Z(\nu_\ell \bar{\nu}_\ell)$ channel also the QCD corrections are constant and at the level of 20%. For the $W^\pm(\ell^\pm\nu_\ell)$ channel the QCD corrections increase up to 30% for small rapidity separation. In actual analyses for VBF-V production and invisible-Higgs searches often tighter requirements on $\Delta\eta_{\mathrm{j_1j_2}}$ than the here considered $\Delta\eta_{\mathrm{j_1j_2}} > 2.5$ are imposed. This will further increase the level of correlation between the $W^\pm(\ell^\pm\nu_\ell)$ and $Z(\nu_\ell\bar{\nu}_\ell)$ channels. Thus correlation uncertainties derived here and then applied with tighter $\Delta\eta_{\mathrm{j_1j_2}}$ requirements can be seen as conservative.

4.3 Precise predictions and uncertainties for $V + 2$ jet ratios

In this section we present predictions and theoretical uncertainties for the ratios of eq. (3.5) between the $m_{\mathrm{j_1j_2}}$ distributions in $pp \to Z(\nu_\ell\bar{\nu}_\ell) + 2\,\mathrm{jets}$ and $pp \to W^\pm(\ell^\pm\nu_\ell) + 2\,\mathrm{jets}$. Numerical predictions for these process ratios and the related uncertainties can be found at [88], where also additional ratios between $pp \to Z(\ell^+\ell^-) + 2\,\mathrm{jets}$ and $pp \to W^\pm(\ell^\pm\nu_\ell) + 2\,\mathrm{jets}$ distributions are available.

The Z/W ratios are the key ingredients of the reweighting procedure defined in eq. (3.8). As nominal theory predictions we take the fixed-order NLO QCD$\times$EW ratios

$$R^{Z/W,M}_{\mathrm{TH}}(x, \vec{\varepsilon}^{\,Z/W,M}_{\mathrm{TH}}) = \frac{\frac{\mathrm{d}}{\mathrm{d}x}\sigma^{Z,M}_{\mathrm{NLO\,QCD\times EW}}(\vec{\varepsilon}^{\,Z,M}_{\mathrm{TH}})}{\frac{\mathrm{d}}{\mathrm{d}x}\sigma^{W,M}_{\mathrm{NLO\,QCD\times EW}}(\vec{\varepsilon}^{\,W,M}_{\mathrm{TH}})}\,, \tag{4.7}$$

where $x = m_{\mathrm{j_1j_2}}$ is the dijet invariant mass. As discussed in section 3, theory uncertainties are described by the nuisance parameters $\vec{\varepsilon}^{\,Z/W,M}_{\mathrm{TH}}$, which are directly acting on the Z/W ratios, combining the uncertainties of the individual processes and their correlations. With this approach, our complete predictions with uncertainties read

$$R^{Z/W,M}_{\mathrm{TH}}(x, \vec{\varepsilon}^{\,Z/W,M}_{\mathrm{TH}}) := R^{Z/W,M}_{\mathrm{TH}}(x) + \sum_i \varepsilon^{Z/W,M}_{i,\mathrm{TH}}\;\delta R^{Z/W,M}_{i,\mathrm{TH}}(x)\,, \tag{4.8}$$

where the nuisance parameters $\varepsilon^{Z/W,M}_{i,\mathrm{TH}}$ are defined as in eq. (3.3) and are meant to be constrained by data in the context of VBF-Higgs analyses as detailed in section 3. In the following we focus on the $\delta R^{Z/W,M}_{i,\mathrm{TH}}(x)$ factors, which encode the various sources of theory uncertainty, as defined in eqs. (4.9)–(4.14). Note that for the two $V+2\,$jet production modes (M), i.e. for QCD and EW production, we define two independent ratios and uncertainties.

To account for unknown QCD corrections beyond NLO in a conservative way, we avoid using scale uncertainties and, following ref. [20], we handle the difference between LO QCD and NLO QCD ratios as uncertainty. More precisely, we consider the effect of switching off NLO QCD corrections in our nominal NLO QCD$\times$EW predictions,

$$\delta R^{Z/W,M}_{\mathrm{QCD}}(x) := \left| R^{Z/W,M}_{\mathrm{NLO\,EW}}(x) - R^{Z/W,M}_{\mathrm{NLO\,QCD\times EW}}(x) \right|\,. \tag{4.9}$$

While this approach effectively downgrades the known NLO QCD corrections to an uncertainty, the bulk of the QCD corrections cancel in the ratio, and the uncertainty $\delta R^{Z/W,M}_{\mathrm{QCD}}$ remains quite small.

For parton showering and NLO matching, in analogy with (2.7) we introduce the factorised combination of NLOPS QCD predictions and EW corrections,

$$\frac{\mathrm{d}}{\mathrm{d}x}\sigma^{V,M}_{\mathrm{NLOPS\,QCD\times EW}} = \frac{\mathrm{d}}{\mathrm{d}x}\sigma^{V,M}_{\mathrm{NLOPS\,QCD}}\left(1 + \kappa^{V,M}_{\mathrm{EW}}(x)\right)\,, \tag{4.10}$$

and as uncertainty we use

$$\delta R^{Z/W,M}_{\rm PS}(x) := \left| R^{Z/W,M}_{\rm NLOPS\, QCD\times EW}(x) - R^{Z/W,M}_{\rm NLO\, QCD\times EW}(x) \right| , \tag{4.11}$$

i.e. the full difference between fixed-order NLO and NLOPS predictions.

To describe the effect of unknown mixed QCD-EW uncertainties beyond NLO we introduce the uncertainty

$$\delta R^{Z/W,M}_{\rm mix}(x) := \left| R^{Z/W,M}_{\rm NLO\, QCD+EW}(x) - R^{Z/W,M}_{\rm NLO\, QCD\times EW}(x) \right| , \tag{4.12}$$

which corresponds to the difference between the additive and multiplicative combination of NLO QCD and NLO EW corrections. Also this prescription can be regarded as a conservative estimate since the multiplicative combination is expected to provide a correct description of the dominant mixed QCD-EW effects beyond NLO.

In case a jet veto is applied to the experimental analysis, also the following uncertainty should be considered,

$$\delta R^{Z/W,M}_{\rm veto}(x) := \left| R^{Z/W,M}_{\rm TH,veto}(x) - R^{Z/W,M}_{\rm NLO\, QCD\times EW}(x) \right| , \tag{4.13}$$

where the ratio $R^{Z/W,M}_{\rm TH,veto}$ is computed in the presence of the "theoretical" veto detailed in eq. (3.12). Note that the effect of the veto cancels to a large extent in the ratio. Thus the prescription of eq. (3.12) does not need to be identical to the veto that is employed in the experimental analysis.

In a situation where in the actual experimental analysis additional requirements on $\Delta\phi_{\rm j_1j_2}$ are imposed a further uncertainty capturing the non-negligible $\Delta\phi_{\rm j_1j_2}$ dependence of QCD higher-order effects in the EW production modes (see section 4.3.2) should be considered for a reliable estimate of non-correlation effects in the Z/W ratio. To this end we split the phase space into the $N = 3$ $\Delta\phi_{\rm j_1j_2}$ bins Φ_i defined in eq. (3.13). Based on these $\Delta\phi_{\rm j_1j_2}$ bins there are two options to determine an additional uncertainty. On the one hand, alternative reweightings within the individual $\Delta\phi_{\rm j_1j_2}$ bins can be performed, and the resulting spread should be considered as an uncertainty. On the other hand, a conservative uncertainty can be defined as

$$\delta R^{Z/W,M}_{\Delta\phi}(x) := \max_{\Phi_i} \left(\left| R^{Z/W,M}_{\rm NLO\, QCD\times EW}\Big|_{\Phi_i} - R^{Z/W,M}_{\rm NLO\, QCD\times EW}(x) \right| \right) . \tag{4.14}$$

In other words, the maximal spread with respect to the nominal ratio of eq. (4.7) in $\Delta\phi_{\rm j_1j_2}$ space is taken as uncertainty of the one-dimensional reweighting procedure. As alternative to the above uncertainties, a two-dimensional reweighting in $\Delta\phi_{\rm j_1j_2}$ and $m_{\rm j_1j_2}$ might be beneficial. However, as shown below in section 4.3.2, at large $m_{\rm j_1j_2}$ i.e. for $m_{\rm j_1j_2} > 2\,$TeV, $\Delta\phi_{\rm j_1j_2}$ variations are small and any non-correlation effects can reliably estimated via any of the two uncertainty prescriptions discussed above. For $m_{\rm j_1j_2} < 2\,$TeV, $\Delta\phi_{\rm j_1j_2}$ variations can be significantly larger, however in this regime the QCD mode anyhow dominates over the EW mode. Therefore, a discussion of two-dimensional reweightings and related uncertainty prescriptions is left to future work.

JHEP01(2023)070

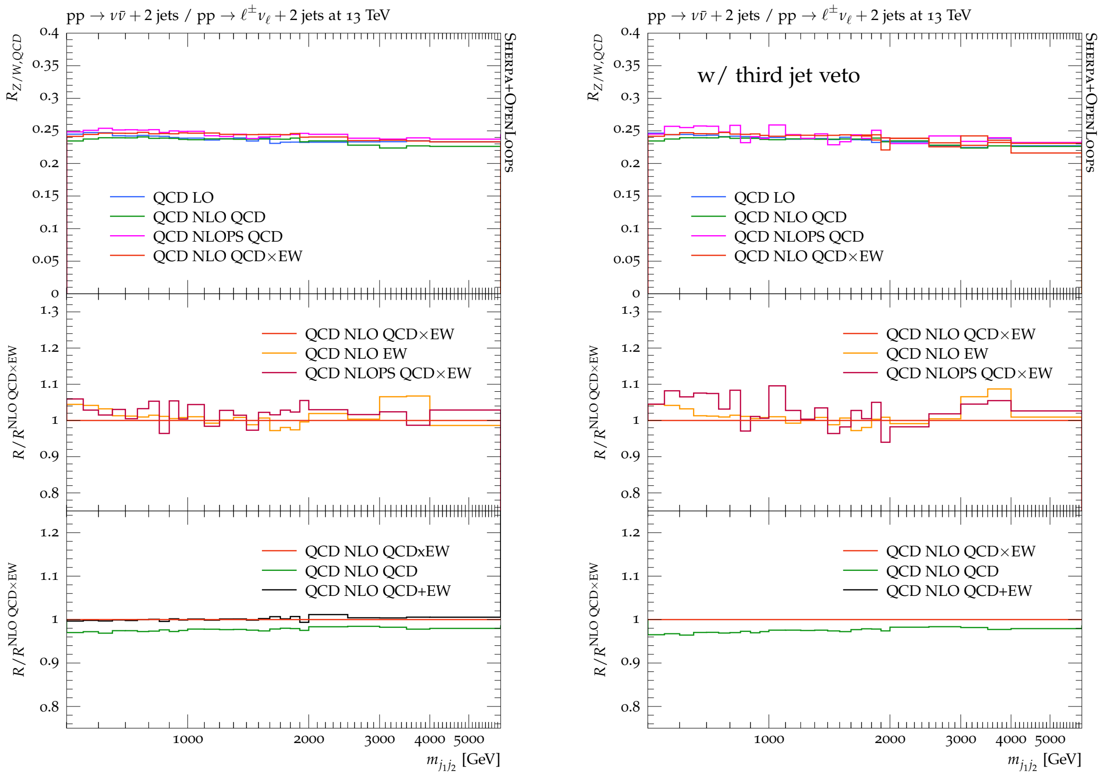

Figure 12. Ratios of the QCD $pp \to Z(\nu_\ell\bar{\nu}_\ell)+2\,\mathrm{jets}$ and QCD $pp \to W^{\pm}(\ell^{\pm}\nu_\ell)+2\,\mathrm{jets}$ distributions in $m_{\mathrm{j_1j_2}}$ inclusive (left) and in the presence of the dynamic veto of eq. (3.12) against a third jet (right). The upper panels compare absolute predictions at LO (blue), NLO QCD (green), NLOPS QCD (magenta) and NLO QCD×EW (red) accuracy. The impact of QCD corrections is illustrated in the middle panel, which shows the relative variation w.r.t. the nominal NLO QCD×EW prediction (red) when switching on the parton shower (NLOPS QCD×EW , purple) or switching off QCD corrections (NLO EW, orange). Similarly, the lowest panel shows the relative effect of switching off EW corrections (NLO QCD, green) or replacing the multiplicative by the additive combination of QCD and EW corrections (NLO QCD+EW, black).

Finally, also PDF uncertainties should be considered. In this case, PDF variations in the numerator and denominator of the Z/W ratio should be correlated. In the following subsections we present predictions for the ratios defined in eq. (4.7) and for the various ingredients that enter the theoretical uncertainties of eqs. (4.8)–(4.14).

4.3.1 Z/W ratios for the QCD production mode

As observed in section 4.2.2, the QCD and EW corrections to the QCD production modes of the individual $Z + 2\,\mathrm{jet}$ and $W + 2\,\mathrm{jet}$ processes are strongly correlated. This is confirmed by the smallness of the corrections in the Z/W ratios shown in figures 12–13.

The left and right plots of figure 12 present the ratio of $m_{\mathrm{j_1j_2}}$-distributions with the inclusive selection cuts, defined in eq. (3.10), and in the presence of the additional jet veto, defined in eq. (3.12). The value of the ratio is around 0.24 and remains almost constant in the considered $m_{\mathrm{j_1j_2}}$ range from 500 to 5000 GeV. The size of the QCD and PS corrections

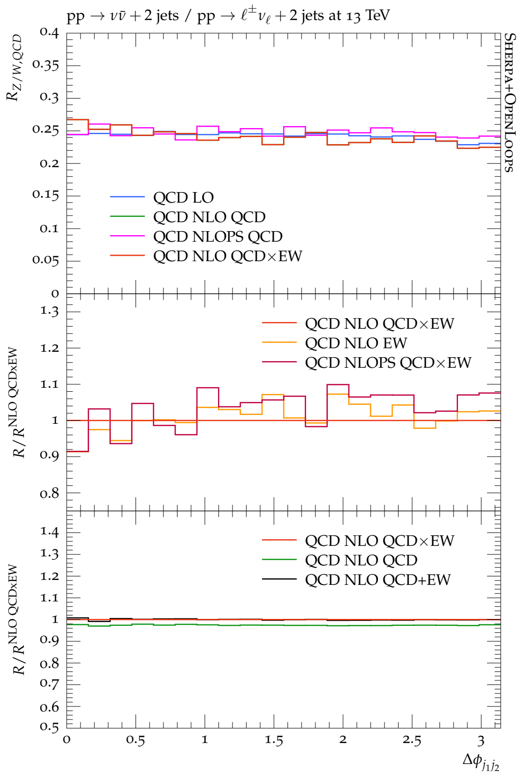

Figure 13. Ratios of the QCD $pp \to Z(\nu_\ell \bar{\nu}_\ell)+2\,$jets and QCD $pp \to W^\pm(\ell^\pm \nu_\ell)+2\,$jets distributions in $\Delta\phi_{\mathrm{j_1 j_2}}$. The same higher-order predictions and conventions as in figure 12 are used.

that enter the uncertainties of eqs. (4.9)–(4.11) is shown in the middle panels. In the inclusive selection NLO QCD corrections to the ratio remain below 4–6% in the entire $m_{\mathrm{j_1 j_2}}$ range, and PS corrections remain below 6%. When the jet veto is applied, in spite of the drastic suppression of the individual $Z + 2\,$jet and $W + 2\,$jet cross sections, the Z/W ratio remains remarkably stable at the percent level. The jet-veto uncertainty of eq. (4.13) is thus quite small. Also the QCD and PS corrections to the ratio are largely insensitive to the jet veto.

As shown in the lowest frames of figure 12, the EW corrections to the QCD Z/W ratio are around 2% and almost independent of $m_{\mathrm{j_1 j_2}}$, both for the inclusive selection and including a jet veto. Due to the strong cancellation of QCD and EW corrections in the ratio, the difference between the additive and multiplicative NLO QCD-EW combinations, which enters the uncertainty of eq. (4.12), is completely negligible.

In figure 13 we present the QCD Z/W ratio for the distributions in $\Delta\phi_{\mathrm{j_1 j_2}}$ without applying a jet veto. Note that, as a result of the acceptance cuts, eq. (3.10), these $\Delta\phi_{\mathrm{j_1 j_2}}$ distributions are dominated by events with $500\,\mathrm{GeV} < m_{\mathrm{j_1 j_2}} < 1500\,\mathrm{GeV}$. The results thus feature a very small dependence on $\Delta\phi_{\mathrm{j_1 j_2}}$, both for the nominal ratio, as well as for the individual corrections. This observation supports the one-dimensional $m_{\mathrm{j_1 j_2}}$-reweighting procedure proposed in section 3, and the $\Delta\phi_{\mathrm{j_1 j_2}}$-uncertainty of eq. (4.14) can be neglected for the QCD production modes.

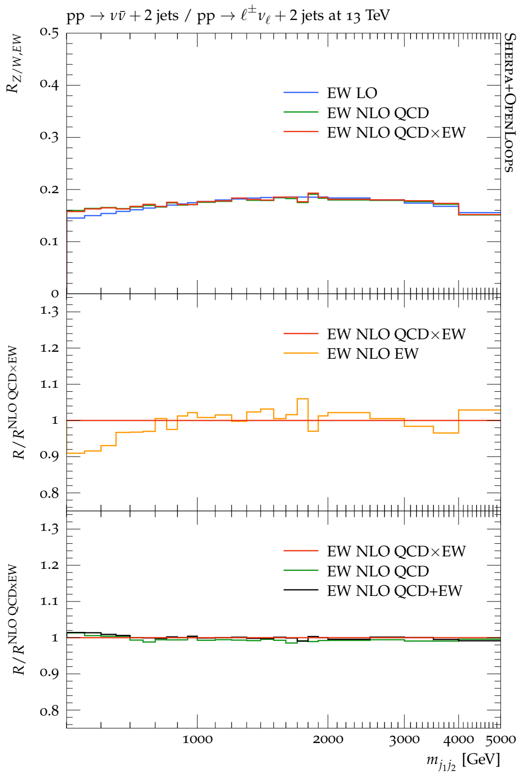

Figure 14. Ratios of the EW $pp \to Z(\nu_\ell\bar{\nu}_\ell) + 2\,\mathrm{jets}$ and EW $pp \to W^\pm(\ell^\pm\nu_\ell) + 2\,\mathrm{jets}$ distributions in $m_{\mathrm{j_1j_2}}$ inclusive (left) and in the presence of the dynamic veto of eq. (3.12) against a third jet (right). Same higher-order predictions and conventions as in figure 12, but without matching to the parton shower.

4.3.2 Z/W ratios for the EW production mode

Higher-order predictions for the ratios of distributions in EW $Z + 2\,\mathrm{jet}$ and EW $W + 2\,\mathrm{jet}$ production are presented in figures 14–16. The left and right plots of figure 14 show the ratio of $m_{\mathrm{j_1j_2}}$-distributions with inclusive selection cuts and in the presence of the additional jet veto. The EW Z/W ratio is around 0.15 and remains rather stable when $m_{\mathrm{j_1j_2}}$ grows from 500 GeV to 5 TeV.

In the absence of the jet veto, as expected from the findings of section 4.2.3, the ratio is quite stable with respect to higher-order corrections. In particular, for $m_{\mathrm{j_1j_2}} > 1\,\mathrm{TeV}$, which corresponds to the most relevant region for invisible-Higgs searches, QCD corrections are at the percent level. Below 1 TeV the QCD corrections tend to become more significant reaching +10% at $m_{\mathrm{j_1j_2}} = 500\,\mathrm{GeV}$. The impact of EW corrections on the inclusive ratio does not exceed 1% in the plotted $m_{\mathrm{j_1j_2}}$ range, and the mixed QCD-EW uncertainties of eq. (4.12) are negligible.

In the presence of the jet veto, the QCD corrections become rather sizeable below 1 TeV and reach the level of +50% at 500 GeV. As a consequence, also mixed QCD-EW uncertainties are somewhat enhanced. This non-universal behaviour of the QCD corrections leads to an enhancement of the QCD uncertainty, as defined in eq. (4.9). However, we note

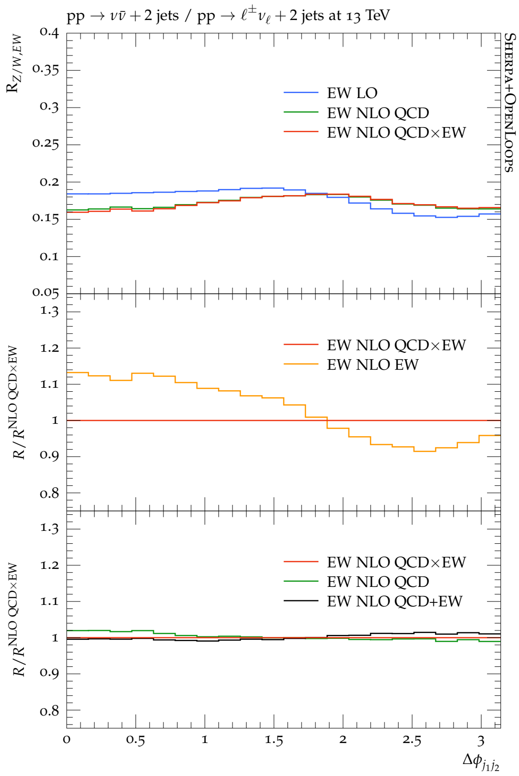

Figure 15. Ratios of the EW $pp \to Z(\nu_\ell\bar{\nu}_\ell) + 2\,\text{jets}$ and EW $pp \to W^\pm(\ell^\pm\nu_\ell) + 2\,\text{jets}$ distributions in $\Delta\phi_{\mathrm{j}_1\mathrm{j}_2}$ without jet veto. Same higher-order predictions and conventions as in figure 12.

that the non-universality of the EW production modes at $m_{\mathrm{j}_1\mathrm{j}_2} < 1\,\text{TeV}$ tends to be washed out by the dominance of the QCD production modes, where all correction effects feature a high degree of universality. Moreover, we point out that the prescription of eq. (4.9) is very conservative and may be replaced by a more realistic estimate if QCD uncertainties play a critical role.

Together with their non-universal behaviour at $m_{\mathrm{j}_1\mathrm{j}_2} < 1\,\text{TeV}$, the QCD corrections to the EW Z/W ratio feature also a nontrivial dependence on $\Delta\phi_{\mathrm{j}_1\mathrm{j}_2}$. This is illustrated in figure 15, where we plot the ratio of the $\Delta\phi_{\mathrm{j}_1\mathrm{j}_2}$ distributions for EW $Z + 2\,$jet and EW $W + 2\,$jet production. The $\Delta\phi_{\mathrm{j}_1\mathrm{j}_2}$ dependence of this ratio features variations at the level of 20% at LO and 15% at NLO QCD×EW . The EW corrections are very small, and their dependence on $\Delta\phi_{\mathrm{j}_1\mathrm{j}_2}$ does not exceed 1%. In contrast, the impact of QCD corrections on the ratio ranges from -10% at small $\Delta\phi_{\mathrm{j}_1\mathrm{j}_2}$ to $+10\%$ around $\Delta\phi_{\mathrm{j}_1\mathrm{j}_2} = 2.5$.

In order to account for this $\Delta\phi_{\mathrm{j}_1\mathrm{j}_2}$ dependence in the reweighting of the one-dimensional $m_{\mathrm{j}_1\mathrm{j}_2}$ distribution we split the phase space into the three $\Delta\phi_{\mathrm{j}_1\mathrm{j}_2}$ bins defined in eq. (3.13). The ratios of $m_{\mathrm{j}_1\mathrm{j}_2}$ distributions for EW $Z + 2\,$jet and EW $W + 2\,$jet production in these three $\Delta\phi_{\mathrm{j}_1\mathrm{j}_2}$ bins are shown in figure 16. For $m_{\mathrm{j}_1\mathrm{j}_2} > 2\,\text{TeV}$, in all three $\Delta\phi_{\mathrm{j}_1\mathrm{j}_2}$-bins we observe very small QCD corrections at the one-percent level, consistently with the behaviour of the inclusive $m_{\mathrm{j}_1\mathrm{j}_2}$ distribution in figure 14. This is due both to the moderate size of the QCD corrections to the individual EW $Z + 2\,$jet and $W + 2\,$jet cross sections (see figure 8)

JHEP01(2023)070

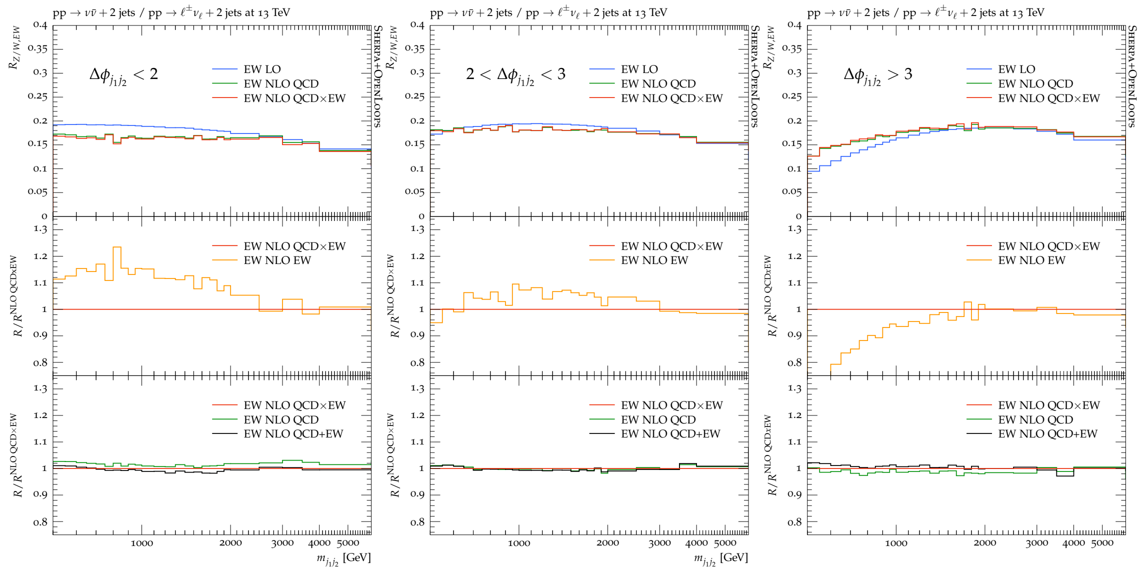

Figure 16. Ratios of the EW $pp \to Z(\nu_\ell\bar{\nu}_\ell) + 2\,\mathrm{jets}$ and EW $pp \to W^\pm(\ell^\pm\nu_\ell) + 2\,\mathrm{jets}$ distributions in $m_{\mathrm{j_1j_2}}$ without jet veto in the regions $\Delta\phi_{\mathrm{j_1j_2}} < 1$ (left), $1 < \Delta\phi_{\mathrm{j_1j_2}} < 2$ (middle), and $\Delta\phi_{\mathrm{j_1j_2}} > 2$ (right). Same higher-order predictions and conventions as in figure 12, but without matching to the parton shower.

and to their strong correlation. In constrast, for $500\,\mathrm{GeV} < m_{\mathrm{j_1j_2}} < 2\,\mathrm{TeV}$ the size of the QCD corrections and their dependence on $\Delta\phi_{\mathrm{j_1j_2}}$ are quite significant. With decreasing $m_{\mathrm{j_1j_2}}$ the impact of the QCD corrections can grow up the level of $+10\%$ or -20%, depending on $\Delta\phi_{\mathrm{j_1j_2}}$. Also the nominal NLO QCD×EW ratio features a non-negligible dependence on $\Delta\phi_{\mathrm{j_1j_2}}$. In order to account for the uncertainties associated with this nontrivial $m_{\mathrm{j_1j_2}}$ and $\Delta\phi_{\mathrm{j_1j_2}}$ dependence, the high-order QCD uncertainty for the inclusive $m_{\mathrm{j_1j_2}}$ distribution, defined in eq. (4.9), is complemented by the additional uncertainty of eq. (4.14), which accounts for the variation of the nomimal ratio in the different $\Delta\phi_{\mathrm{j_1j_2}}$ bins.

5 Conclusions

The precise control of SM backgrounds is key in order to harness the full potential of invisible-Higgs searches in the VBF production mode at the LHC. Irreducible background contributions to the corresponding signature of missing transverse energy plus two jets with high invariant mass arise from the SM processes $pp \to Z(\nu_\ell\bar{\nu}_\ell) + 2\,\mathrm{jets}$ and $pp \to W^\pm(\ell^\pm\nu_\ell) + 2\,\mathrm{jets}$, where the lepton is outside of the acceptance region. Such backgrounds can be predicted with rather good theoretical accuracy in perturbation theory, while the residual theoretical uncertainties can be further reduced with a data-driven approach. In particular, the irreducible $pp \to Z(\nu_\ell\bar{\nu}_\ell) + 2\,\mathrm{jets}$ background can be constrained by means of accurate data for $pp \to W^\pm(\ell^\pm\nu_\ell) + 2\,\mathrm{jets}$ with a visible lepton, in combination with precise theoretical predictions for the correlation between $Z + 2\,\mathrm{jet}$ and $W + 2\,\mathrm{jet}$ production.

JHEP01(2023)070

In this article we have presented parton-level predictions including complete NLO QCD and EW corrections for all relevant $V+2$ jet processes in the SM. These reactions involve various perturbative contributions, which can be split into QCD modes, EW modes, and interference contributions. For the first time we have consistently computed all four perturbative contributions to $Z+2$ jet and $W+2$ jet production that arise at NLO QCD+EW without applying any approximations. Based on the observation that the LO interference between the QCD and EW modes is very small, the NLO contributions of $\mathcal{O}(\alpha_s^3\alpha^2)$ and $\mathcal{O}(\alpha_s^2\alpha^3)$ can be regarded as QCD and EW corrections to the QCD production mode, while $\mathcal{O}(\alpha_s\alpha^4)$ and $\mathcal{O}(\alpha^5)$ correspond to QCD and EW corrections to the EW production mode. In the signal region for invisible-Higgs searches, i.e. at large dijet invariant mass, $m_{j_1j_2}$, the EW $V+2$ jet production mode is dominated by VBF topologies, but our calculations account for all possible $V+2$ jet topologies, including contributions that correspond to diboson production with semi-leptonic decays, as well as single-top production and decay in the s-, t- and Wt-channels.

The QCD corrections to the EW modes are small at large $m_{j_1j_2}$, while the EW corrections can reach up to -20%. Both for the QCD and the EW modes, we have found a high degree of correlation between the higher-order QCD and EW corrections to $pp \to Z(\nu_\ell\bar{\nu}_\ell)+2$ jets and $pp \to W^\pm(\ell^\pm\nu_\ell)+2$ jets. As a result of this strong correlation, higher-order corrections and uncertainties cancel to a large extent in the ratio of $pp \to Z(\nu_\ell\bar{\nu}_\ell)+2$ jets and $pp \to W^\pm(\ell^\pm\nu_\ell)+2$ jets cross sections. Based on this observation we have proposed to exploit precise theoretical predictions for this Z/W ratio in combination with data in order to control the $V+2$ jet backgrounds to invisible-Higgs searches with few-percent precision. To this end we have provided an explicit recipe, based on the reweighting of $m_{j_1j_2}$ distributions, which can be applied to the Monte Carlo samples that are used in the experimental analyses. This reweighting is implemented at the level of the QCD and EW Z/W ratios, such as to exploit the very small theoretical uncertainties in these observables.

In the phase space relevant for invisible-Higgs searches, at $m_{j_1j_2} > 1$ TeV, the correlation of higher-order corrections in $Z+2$ jet and $W+2$ jet production turns out to be particular strong, and theoretical uncertainties in the Z/W ratios are as small as a few percent. Moderate decorrelation effects have been observed at smaller $m_{j_1j_2}$ in the ratio of the EW production modes. Such effects can reach up to 10% in the ratio. They are driven by non-universal QCD corrections to the EW $V+2$ jet production modes, and they originate from semileptonic diboson topologies and single-top contributions that are not included in the naive VBF approximation. The Z/W correlation can in principle be further enhanced separating these non-universal contributions. We leave this to future investigation.

Based on the predictions and uncertainties derived in this article significant sensitivity improvements can be expected in searches for invisible Higgs decays. In fact, our predictions and the proposed reweighting procedure have already been applied in a recent ATLAS search [89] yielding an upper limit of 14.5% on the invisible branching ratio of the Higgs at 95% confidence level. In this context the search presented in [89] also provides a closure test of the reweighting procedure introduced here. The approach and the theoretical predictions presented in this paper can also be applied to measurements of $V+2$ jet production via VFB in order to derive constraints on effective field theories beyond the Standard Model.

Acknowledgments

We thank Lorenzo Mai for useful discussions and cross-checks. We also thank Christian Gütschow for useful discussions and comments on the manuscript. J.M.L. is supported by the Science and Technology Research Council (STFC) under the Consolidated Grant ST/T00102X/1 and the STFC Ernest Rutherford Fellowship ST/S005048/1. M.S. is supported by the Royal Society through a University Research Fellowship (URF\R1\180549) and an Enhancement Award (RGF\EA\181033, CEC19\100349, and RF\ERE\210397). The work of S.P. was supported by the Swiss National Science Foundation (SNSF) under contract BSCGI0-157722. We acknowledge the use of the DiRAC Cumulus HPC facility under Grant No. PPSP226.

References

[1] A. Denner, S. Dittmaier and A. Mück, *PROPHECY4F 3.0: A Monte Carlo program for Higgs-boson decays into four-fermion final states in and beyond the Standard Model*, *Comput. Phys. Commun.* **254** (2020) 107336 [arXiv:1912.02010] [INSPIRE].

[2] R.E. Shrock and M. Suzuki, *Invisible Decays of Higgs Bosons*, *Phys. Lett. B* **110** (1982) 250 [INSPIRE].

[3] D. Choudhury and D.P. Roy, *Signatures of an invisibly decaying Higgs particle at LHC*, *Phys. Lett. B* **322** (1994) 368 [hep-ph/9312347] [INSPIRE].

[4] D. Dominici and J.F. Gunion, *Invisible Higgs Decays from Higgs Graviscalar Mixing*, *Phys. Rev. D* **80** (2009) 115006 [arXiv:0902.1512] [INSPIRE].

[5] G. Bélanger, F. Boudjema, A. Cottrant, R.M. Godbole and A. Semenov, *The MSSM invisible Higgs in the light of dark matter and $g-2$*, *Phys. Lett. B* **519** (2001) 93 [hep-ph/0106275] [INSPIRE].

[6] A. Djouadi, O. Lebedev, Y. Mambrini and J. Quevillon, *Implications of LHC searches for Higgs-portal dark matter*, *Phys. Lett. B* **709** (2012) 65 [arXiv:1112.3299] [INSPIRE].

[7] S. Baek, P. Ko, W.-I. Park and E. Senaha, *Higgs Portal Vector Dark Matter: Revisited*, *JHEP* **05** (2013) 036 [arXiv:1212.2131] [INSPIRE].

[8] L. Calibbi, J.M. Lindert, T. Ota and Y. Takanishi, *Cornering light Neutralino Dark Matter at the LHC*, *JHEP* **10** (2013) 132 [arXiv:1307.4119] [INSPIRE].

[9] A. Beniwal et al., *Combined analysis of effective Higgs portal dark matter models*, *Phys. Rev. D* **93** (2016) 115016 [arXiv:1512.06458] [INSPIRE].

[10] A. Butter, T. Plehn, M. Rauch, D. Zerwas, S. Henrot-Versillé and R. Lafaye, *Invisible Higgs Decays to Hooperons in the NMSSM*, *Phys. Rev. D* **93** (2016) 015011 [arXiv:1507.02288] [INSPIRE].

[11] S. Argyropoulos, O. Brandt and U. Haisch, *Collider Searches for Dark Matter through the Higgs Lens*, *Symmetry* **13** (2021) 2406 [arXiv:2109.13597] [INSPIRE].

[12] ATLAS collaboration, *Search for an invisibly decaying Higgs boson or dark matter candidates produced in association with a Z boson in pp collisions at* $\sqrt{s} = 13$ *TeV with the ATLAS detector*, Phys. Lett. B **776** (2018) 318 [arXiv:1708.09624] [INSPIRE].

[13] ATLAS collaboration, *Search for invisible Higgs boson decays in vector boson fusion at* $\sqrt{s} = 13$ *TeV with the ATLAS detector*, Phys. Lett. B **793** (2019) 499 [arXiv:1809.06682] [INSPIRE].

[14] ATLAS collaboration, *Search for dark matter in events with a hadronically decaying vector boson and missing transverse momentum in pp collisions at* $\sqrt{s} = 13$ *TeV with the ATLAS detector*, JHEP **10** (2018) 180 [arXiv:1807.11471] [INSPIRE].

[15] ATLAS collaboration, *Combination of searches for invisible Higgs boson decays with the ATLAS experiment*, Phys. Rev. Lett. **122** (2019) 231801 [arXiv:1904.05105] [INSPIRE].

[16] CMS collaboration, *Search for invisible decays of Higgs bosons in the vector boson fusion and associated ZH production modes*, Eur. Phys. J. C **74** (2014) 2980 [arXiv:1404.1344] [INSPIRE].

[17] CMS collaboration, *Searches for invisible decays of the Higgs boson in pp collisions at* $\sqrt{s} = 7$*, 8, and 13 TeV*, JHEP **02** (2017) 135 [arXiv:1610.09218] [INSPIRE].

[18] CMS collaboration, *Search for invisible decays of a Higgs boson produced through vector boson fusion in proton-proton collisions at* $\sqrt{s} = 13$ *TeV*, Phys. Lett. B **793** (2019) 520 [arXiv:1809.05937] [INSPIRE].

[19] CMS collaboration, *Search for invisible decays of the Higgs boson produced via vector boson fusion in proton-proton collisions at* $\sqrt{s} = 13$ *TeV*, Phys. Rev. D **105** (2022) 092007 [arXiv:2201.11585] [INSPIRE].

[20] J.M. Lindert et al., *Precise predictions for V+ jets dark matter backgrounds*, Eur. Phys. J. C **77** (2017) 829 [arXiv:1705.04664] [INSPIRE].

[21] ATLAS collaboration, *Search for new phenomena in events with an energetic jet and missing transverse momentum in pp collisions at* $\sqrt{s} = 13$ *TeV with the ATLAS detector*, Phys. Rev. D **103** (2021) 112006 [arXiv:2102.10874] [INSPIRE].

[22] CMS collaboration, *Search for new particles in events with energetic jets and large missing transverse momentum in proton-proton collisions at* $\sqrt{s} = 13$ *TeV*, JHEP **11** (2021) 153 [arXiv:2107.13021] [INSPIRE].

[23] ATLAS collaboration, *Measurement of the electroweak production of dijets in association with a Z-boson and distributions sensitive to vector boson fusion in proton-proton collisions at* $\sqrt{s} = 8$ *TeV using the ATLAS detector*, JHEP **04** (2014) 031 [arXiv:1401.7610] [INSPIRE].

[24] CMS collaboration, *Measurement of electroweak production of a W boson and two forward jets in proton-proton collisions at* $\sqrt{s} = 8$ *TeV*, JHEP **11** (2016) 147 [arXiv:1607.06975] [INSPIRE].

[25] ATLAS collaboration, *Measurement of the cross-section for electroweak production of dijets in association with a Z boson in pp collisions at* $\sqrt{s} = 13$ *TeV with the ATLAS detector*, Phys. Lett. B **775** (2017) 206 [arXiv:1709.10264] [INSPIRE].

[26] ATLAS collaboration, *Measurements of electroweak Wjj production and constraints on anomalous gauge couplings with the ATLAS detector*, Eur. Phys. J. C **77** (2017) 474 [arXiv:1703.04362] [INSPIRE].

[27] CMS collaboration, *Electroweak production of two jets in association with a Z boson in proton-proton collisions at $\sqrt{s} = 13$ TeV*, *Eur. Phys. J. C* **78** (2018) 589 [arXiv:1712.09814] [INSPIRE].

[28] J.M. Campbell and R.K. Ellis, *Next-to-Leading Order Corrections to $W + 2$ jet and $Z + 2$ Jet Production at Hadron Colliders*, *Phys. Rev. D* **65** (2002) 113007 [hep-ph/0202176] [INSPIRE].

[29] F. Febres Cordero, L. Reina and D. Wackeroth, *NLO QCD corrections to W boson production with a massive b-quark jet pair at the Tevatron $p\bar{p}$ collider*, *Phys. Rev. D* **74** (2006) 034007 [hep-ph/0606102] [INSPIRE].

[30] J.M. Campbell et al., *Associated Production of a W Boson and One b Jet*, *Phys. Rev. D* **79** (2009) 034023 [arXiv:0809.3003] [INSPIRE].

[31] C.F. Berger et al., *Precise Predictions for $W + 3$ Jet Production at Hadron Colliders*, *Phys. Rev. Lett.* **102** (2009) 222001 [arXiv:0902.2760] [INSPIRE].

[32] R.K. Ellis, K. Melnikov and G. Zanderighi, *Generalized unitarity at work: first NLO QCD results for hadronic W^+ 3jet production*, *JHEP* **04** (2009) 077 [arXiv:0901.4101] [INSPIRE].

[33] R.K. Ellis, K. Melnikov and G. Zanderighi, *$W + 3$ jet production at the Tevatron*, *Phys. Rev. D* **80** (2009) 094002 [arXiv:0906.1445] [INSPIRE].

[34] C.F. Berger et al., *Next-to-Leading Order QCD Predictions for W+3-Jet Distributions at Hadron Colliders*, *Phys. Rev. D* **80** (2009) 074036 [arXiv:0907.1984] [INSPIRE].

[35] C.F. Berger et al., *Precise Predictions for $W + 4$ Jet Production at the Large Hadron Collider*, *Phys. Rev. Lett.* **106** (2011) 092001 [arXiv:1009.2338] [INSPIRE].

[36] Z. Bern et al., *Next-to-Leading Order $W + 5$-Jet Production at the LHC*, *Phys. Rev. D* **88** (2013) 014025 [arXiv:1304.1253] [INSPIRE].

[37] F.R. Anger, F. Febres Cordero, S. Höche and D. Maître, *Weak vector boson production with many jets at the LHC $\sqrt{s} = 13$ TeV*, *Phys. Rev. D* **97** (2018) 096010 [arXiv:1712.08621] [INSPIRE].

[38] S. Badger, H.B. Hartanto and S. Zoia, *Two-Loop QCD Corrections to $Wb\bar{b}$ Production at Hadron Colliders*, *Phys. Rev. Lett.* **127** (2021) 012001 [arXiv:2102.02516] [INSPIRE].

[39] S. Abreu, F. Febres Cordero, H. Ita, M. Klinkert, B. Page and V. Sotnikov, *Leading-color two-loop amplitudes for four partons and a W boson in QCD*, *JHEP* **04** (2022) 042 [arXiv:2110.07541] [INSPIRE].

[40] E. Re, *NLO corrections merged with parton showers for $Z + 2$ jets production using the POWHEG method*, *JHEP* **10** (2012) 031 [arXiv:1204.5433] [INSPIRE].

[41] J. Alwall et al., *The automated computation of tree-level and next-to-leading order differential cross sections, and their matching to parton shower simulations*, *JHEP* **07** (2014) 079 [arXiv:1405.0301] [INSPIRE].

[42] SHERPA collaboration, *Event Generation with Sherpa 2.2*, *SciPost Phys.* **7** (2019) 034 [arXiv:1905.09127] [INSPIRE].

[43] R. Frederix, S. Frixione, A. Papaefstathiou, S. Prestel and P. Torrielli, *A study of multi-jet production in association with an electroweak vector boson*, *JHEP* **02** (2016) 131 [arXiv:1511.00847] [INSPIRE].

[44] S. Hoeche, F. Krauss, M. Schönherr and F. Siegert, *QCD matrix elements + parton showers: The NLO case*, *JHEP* **04** (2013) 027 [arXiv:1207.5030] [INSPIRE].

JHEP01(2023)070

[45] T. Gehrmann, S. Höche, F. Krauss, M. Schönherr and F. Siegert, *NLO QCD matrix elements + parton showers in $e^+e^- \to$ hadrons*, JHEP **01** (2013) 144 [arXiv:1207.5031] [INSPIRE].

[46] L. Lönnblad and S. Prestel, *Merging Multi-leg NLO Matrix Elements with Parton Showers*, JHEP **03** (2013) 166 [arXiv:1211.7278] [INSPIRE].

[47] R. Frederix and S. Frixione, *Merging meets matching in MC@NLO*, JHEP **12** (2012) 061 [arXiv:1209.6215] [INSPIRE].

[48] J.R. Andersen, T. Hapola and J.M. Smillie, *W Plus Multiple Jets at the LHC with High Energy Jets*, JHEP **09** (2012) 047 [arXiv:1206.6763] [INSPIRE].

[49] J.R. Andersen, J.J. Medley and J.M. Smillie, *Z/γ^* plus multiple hard jets in high energy collisions*, JHEP **05** (2016) 136 [arXiv:1603.05460] [INSPIRE].

[50] J.R. Andersen, J.A. Black, H.M. Brooks, E.P. Byrne, A. Maier and J.M. Smillie, *Combined subleading high-energy logarithms and NLO accuracy for W production in association with multiple jets*, JHEP **04** (2021) 105 [arXiv:2012.10310] [INSPIRE].

[51] A. Denner, L. Hofer, A. Scharf and S. Uccirati, *Electroweak corrections to lepton pair production in association with two hard jets at the LHC*, JHEP **01** (2015) 094 [arXiv:1411.0916] [INSPIRE].

[52] S. Kallweit, J.M. Lindert, P. Maierhöfer, S. Pozzorini and M. Schönherr, *NLO electroweak automation and precise predictions for W + multijet production at the LHC*, JHEP **04** (2015) 012 [arXiv:1412.5157] [INSPIRE].

[53] S. Kallweit, J.M. Lindert, P. Maierhöfer, S. Pozzorini and M. Schönherr, *NLO QCD + EW predictions for V + jets including off-shell vector-boson decays and multijet merging*, JHEP **04** (2016) 021 [arXiv:1511.08692] [INSPIRE].

[54] M. Chiesa, N. Greiner and F. Tramontano, *Automation of electroweak corrections for LHC processes*, J. Phys. G **43** (2016) 013002 [arXiv:1507.08579] [INSPIRE].

[55] C. Oleari and D. Zeppenfeld, *QCD corrections to electroweak $\ell\nu_\ell jj$ and $\ell^+\ell^- jj$ production*, Phys. Rev. D **69** (2004) 093004 [hep-ph/0310156] [INSPIRE].

[56] B. Jager, *Next-to-leading order QCD corrections to photon production via weak-boson fusion*, Phys. Rev. D **81** (2010) 114016 [arXiv:1004.0825] [INSPIRE].

[57] B. Jager, S. Schneider and G. Zanderighi, *Next-to-leading order QCD corrections to electroweak Zjj production in the POWHEG BOX*, JHEP **09** (2012) 083 [arXiv:1207.2626] [INSPIRE].

[58] F. Schissler and D. Zeppenfeld, *Parton Shower Effects on W and Z Production via Vector Boson Fusion at NLO QCD*, JHEP **04** (2013) 057 [arXiv:1302.2884] [INSPIRE].

[59] R. Frederix, D. Pagani and I. Tsinikos, *Precise predictions for single-top production: the impact of EW corrections and QCD shower on the t-channel signature*, JHEP **09** (2019) 122 [arXiv:1907.12586] [INSPIRE].

[60] M. Cacciari, G.P. Salam and G. Soyez, *The anti-k_t jet clustering algorithm*, JHEP **04** (2008) 063 [arXiv:0802.1189] [INSPIRE].

[61] S. Frixione, *Isolated photons in perturbative QCD*, Phys. Lett. B **429** (1998) 369 [hep-ph/9801442] [INSPIRE].

[62] E.W.N. Glover and A.G. Morgan, *Measuring the photon fragmentation function at LEP*, Z. Phys. C **62** (1994) 311 [INSPIRE].

JHEP01(2023)070

[63] A. Denner, S. Dittmaier, M. Pellen and C. Schwan, *Low-virtuality photon transitions $\gamma^* \to f\bar{f}$ and the photon-to-jet conversion function*, *Phys. Lett. B* **798** (2019) 134951 [arXiv:1907.02366] [INSPIRE].

[64] M. Schönherr, *An automated subtraction of NLO EW infrared divergences*, *Eur. Phys. J. C* **78** (2018) 119 [arXiv:1712.07975] [INSPIRE].

[65] S. Frixione and B.R. Webber, *Matching NLO QCD computations and parton shower simulations*, *JHEP* **06** (2002) 029 [hep-ph/0204244] [INSPIRE].

[66] S. Hoeche, F. Krauss, M. Schönherr and F. Siegert, *A critical appraisal of NLO+PS matching methods*, *JHEP* **09** (2012) 049 [arXiv:1111.1220] [INSPIRE].

[67] S. Schumann and F. Krauss, *A Parton shower algorithm based on Catani-Seymour dipole factorisation*, *JHEP* **03** (2008) 038 [arXiv:0709.1027] [INSPIRE].

[68] F. Krauss, R. Kuhn and G. Soff, *AMEGIC++ 1.0: A Matrix element generator in C++*, *JHEP* **02** (2002) 044 [hep-ph/0109036] [INSPIRE].

[69] T. Gleisberg and F. Krauss, *Automating dipole subtraction for QCD NLO calculations*, *Eur. Phys. J. C* **53** (2008) 501 [arXiv:0709.2881] [INSPIRE].

[70] T. Gleisberg et al., *Event generation with SHERPA 1.1*, *JHEP* **02** (2009) 007 [arXiv:0811.4622] [INSPIRE].

[71] S. Catani and M.H. Seymour, *A General algorithm for calculating jet cross-sections in NLO QCD*, *Nucl. Phys. B* **485** (1997) 291 [*Erratum ibid.* **510** (1998) 503] [hep-ph/9605323] [INSPIRE].

[72] S. Catani, S. Dittmaier, M.H. Seymour and Z. Trócsányi, *The Dipole formalism for next-to-leading order QCD calculations with massive partons*, *Nucl. Phys. B* **627** (2002) 189 [hep-ph/0201036] [INSPIRE].

[73] S. Dittmaier, *A General approach to photon radiation off fermions*, *Nucl. Phys. B* **565** (2000) 69 [hep-ph/9904440] [INSPIRE].

[74] S. Dittmaier, A. Kabelschacht and T. Kasprzik, *Polarized QED splittings of massive fermions and dipole subtraction for non-collinear-safe observables*, *Nucl. Phys. B* **800** (2008) 146 [arXiv:0802.1405] [INSPIRE].

[75] T. Gehrmann and N. Greiner, *Photon Radiation with MadDipole*, *JHEP* **12** (2010) 050 [arXiv:1011.0321] [INSPIRE].

[76] F. Buccioni et al., *OpenLoops 2*, *Eur. Phys. J. C* **79** (2019) 866 [arXiv:1907.13071] [INSPIRE].

[77] F. Cascioli, P. Maierhöfer and S. Pozzorini, *Scattering Amplitudes with Open Loops*, *Phys. Rev. Lett.* **108** (2012) 111601 [arXiv:1111.5206] [INSPIRE].

[78] F. Buccioni, S. Pozzorini and M. Zoller, *On-the-fly reduction of open loops*, *Eur. Phys. J. C* **78** (2018) 70 [arXiv:1710.11452] [INSPIRE].

[79] A. Denner and S. Dittmaier, *Scalar one-loop 4-point integrals*, *Nucl. Phys. B* **844** (2011) 199 [arXiv:1005.2076] [INSPIRE].

[80] A. Denner, S. Dittmaier and L. Hofer, *Collier: a fortran-based Complex One-Loop LIbrary in Extended Regularizations*, *Comput. Phys. Commun.* **212** (2017) 220 [arXiv:1604.06792] [INSPIRE].

JHEP01(2023)070

[81] A. van Hameren, *OneLOop: For the evaluation of one-loop scalar functions*, Comput. Phys. Commun. **182** (2011) 2427 [arXiv:1007.4716] [INSPIRE].

[82] A. Denner, S. Dittmaier, M. Roth and D. Wackeroth, *Predictions for all processes* $e^+e^- \to 4$ *fermions* $+ \gamma$, Nucl. Phys. B **560** (1999) 33 [hep-ph/9904472] [INSPIRE].

[83] A. Denner, S. Dittmaier, M. Roth and L.H. Wieders, *Electroweak corrections to charged-current* $e^+e^- \to 4$ *fermion processes: Technical details and further results*, Nucl. Phys. B **724** (2005) 247 [*Erratum ibid.* **854** (2012) 504] [hep-ph/0505042] [INSPIRE].

[84] A. Denner and S. Dittmaier, *Electroweak Radiative Corrections for Collider Physics*, Phys. Rept. **864** (2020) 1 [arXiv:1912.06823] [INSPIRE].

[85] S. Kallweit, J.M. Lindert, S. Pozzorini and M. Schönherr, *NLO QCD+EW predictions for* $2\ell 2\nu$ *diboson signatures at the LHC*, JHEP **11** (2017) 120 [arXiv:1705.00598] [INSPIRE].

[86] A. Manohar, P. Nason, G.P. Salam and G. Zanderighi, *How bright is the proton? A precise determination of the photon parton distribution function*, Phys. Rev. Lett. **117** (2016) 242002 [arXiv:1607.04266] [INSPIRE].

[87] S. Hoeche, F. Krauss, S. Schumann and F. Siegert, *QCD matrix elements and truncated showers*, JHEP **05** (2009) 053 [arXiv:0903.1219] [INSPIRE].

[88] J.M. Lindert, *Public repository with NLO QCD+EW theoretical predictions and uncertainties for V+2jet ratios*, https://gitlab.com/Lindert/vjj.git.

[89] ATLAS collaboration, *Search for invisible Higgs-boson decays in events with vector-boson fusion signatures using* $139\,fb^{-1}$ *of proton-proton data recorded by the ATLAS experiment*, JHEP **08** (2022) 104 [arXiv:2202.07953] [INSPIRE].